Deep-Sea Research I 85 (2014) 15–34

Contents lists available at ScienceDirect

Deep-Sea Research I

journal homepage: www.elsevier.com/locate/dsri

Lipid and ^{13}C signatures of submicron and suspended particulate organic matter in the Eastern Tropical North Pacific: Implications for the contribution of Bacteria

Hilary G. Close [a,*], Stuart G. Wakeham [b,c], Ann Pearson [a]

[a] Department of Earth and Planetary Sciences, Harvard University, Cambridge, MA 02138, USA
[b] Skidaway Institute of Oceanography, Savannah, GA 31411, USA
[c] School of Oceanography, University of Washington, Seattle, WA 98195, USA

ARTICLE INFO

Article history:
Received 15 July 2013
Received in revised form
25 November 2013
Accepted 28 November 2013
Available online 12 December 2013

Keywords:
Particulate organic matter
Carbon isotopes
Lipid biomarkers
Bacteria
Oxygen minimum zone
Eastern Tropical North Pacific

ABSTRACT

The contribution of bacterial biomass to total particulate organic matter (POM) in the ocean, including exported material, is poorly constrained. To examine potential signatures for the presence and export of bacterioplankton and their detrital remains, here we provide a detailed compound-specific ^{13}C characterization of fatty acids from membrane polar lipids obtained from a water column profile in the Eastern Tropical North Pacific. POM of submicron size (0.2–0.7 μm; "X-POM") was sampled and analyzed separately from the size class typically collected as "suspended" POM (0.7–53 μm; "L-POM"). The distributions of polar head group classes, specific fatty acid side chains, and natural ^{13}C contents all vary, both between particle size classes and with depth in the water column. In general, the polar lipids in submicron material – and by inference, lipids of bacterial origin – have higher ^{13}C content than polar lipids from larger POM and are equally abundant. Lipid signatures from the photic zone appear to be partially conserved in the suspended pool during transit down the water column. However, bacterial heterotrophy and possibly chemoautotrophy partially overprint these surface signatures. In addition, active metabolisms in the oxygen minimum zone (OMZ) appear to mediate the disaggregation of POM transported from the surface, thus adding complexity to the pathways of mid-water carbon flux and providing additional organic substrates to the OMZ and below. This "substrate injection" may provide important fuel for the denitrification and anammox reactions. Finally, examination of ^{13}C content in polar lipids provides a basis for new interpretation of depth-related variations in $\delta^{13}C$ values of bulk suspended POM.

1. Introduction

Export of organic matter from the surface ocean is a major flux of carbon into deep reservoirs, removing it from exchange with atmospheric CO_2 on short time-scales. In order to predict carbon cycle responses to global change, it is vital to accurately characterize biotic and environmental controls that affect the balance of export versus respiration. Small plankton and other slowly-settling particles – otherwise known as "suspended" POM – have been overlooked as contributors to carbon export (e.g., Richardson and Jackson, 2007; Lomas and Moran, 2011; Arístegui et al., 2009; Burd et al., 2010; Alonso-González et al., 2010). The majority of cellular biomass in the surface ocean is classified as suspended: most phytoplankton and all free-living Bacteria are smaller than the typical 53 μm cut-off often used for distinguishing "sinking" versus "suspended" POM (Kostandinov et al., 2010; Bacon et al., 1985; Wakeham and Lee, 1989). Because hydrodynamic models dependent on Stokes's Law suggest that this small (<53 μm) material should not sink passively to any extent, the downward flux of suspended POM in the water column must involve other processes.

Recent studies have explored the potential for exchange between "suspended" and "sinking" POM (Sheridan et al., 2002; Goutx et al., 2007; Abramson et al., 2010). Radioisotope tracers indicate significant exchange and hence homogenization between these two pools (Bacon and Anderson, 1982), but organic characterization reveals their compositions to be qualitatively dissimilar (Wakeham and Canuel, 1988; Abramson et al., 2010). Significantly, these previous studies did not include POM $< \sim 1$ μm in diameter ("submicron" POM). However, the majority of free-living marine Bacteria and Archaea exist within the submicron size class (e.g., Koike et al., 1990; Ingalls et al., 2012); these, along with particle-attached prokaryotes, are critical mediators of particle transformations. The biomass of living Bacteria alone comprises $>20\%$ of

* Corresponding author at: Department of Geology and Geophysics, University of Hawaii, Honolulu, HI 96822, USA. Tel.: +1 808 956 7757.
E-mail address: hclose@hawaii.edu (H.G. Close).

0967-0637/$ - see front matter © 2013 Elsevier Ltd. All rights reserved.
http://dx.doi.org/10.1016/j.dsr.2013.11.005

POM in the oligotrophic Pacific surface ocean (Kawasaki et al., 2011), with similar estimates in other oceanic regions (Li et al., 1983; Turley et al., 1986; Fuhrman et al., 1989; Karl et al., 1988; Cho and Azam, 1988; Koike et al., 1990). By routinely neglecting submicron POM in geochemical measurements, key stages in the production, aggregation, disaggregation, and consumption of organic matter may be missing from our conceptual and numerical models of POM export.

Here we begin to address this deficit in knowledge by comparing "submicron" POM (0.2–0.7 μm; henceforth "X" for extra-small) and a typical "suspended" class of POM (0.7–53 μm; "L" for large) from the water column of the Eastern Tropical North Pacific (ETNP). Subsurface waters in the ETNP contain one of the three most extensive oxygen minimum zones (OMZ) in the world ocean (Ward et al., 2008). Export of organic matter at this location has important implications for global productivity: OMZs are the sites of the largest discrete losses of fixed nitrogen from the world ocean (Codispoti et al., 2001). The supply of organic matter to denitrifying Bacteria in the OMZ may be the limiting factor in determining the magnitude of this nitrogen loss (Ward et al., 2008). The global strength and extent of OMZs is increasing with recent climate trends (Stramma et al., 2008), so it is vital to characterize the transformations in POM in these regions.

We focus on the upper 800 m of the water column in the ETNP, encompassing the depths over which the remineralization of exported carbon is the most intensive (Martin et al., 1987; Buesseler et al., 2007). We utilize a compound-specific approach to characterize the concentration and $\delta^{13}C$ values of fatty acids from X-POM and L-POM. Fatty acid data described here derive from two classes of intact polar lipids (IPLs), nominally distinguished as glycolipids and phospholipids. This approach is novel in allowing us to capture the isotopic characteristics of primarily in situ organisms; compound-specific $\delta^{13}C$ values rarely are reported separately for glycolipids versus phospholipids from suspended POM.

The results indicate that *de novo* production by autotrophs and heterotrophs, sinking, and particle dynamics such as aggregation/disaggregation all likely influence the lipid and isotopic content of submicron and larger suspended size classes of POM throughout the water column. Specifically, we show that (i) X-POM and L-POM contain approximately equal concentrations of IPLs; (ii) there is wide heterogeneity in $\delta^{13}C$ values of individual compounds, both within and between samples; (iii) X-POM is enriched in ^{13}C, potentially a bacterial signature; and (iv) there are unique processes and $\delta^{13}C$ signatures associated with the strong OMZ in this region.

2. Methods

Oceanographic stations in the Eastern Tropical North Pacific were defined during a 2007 field season (Cass et al., 2011; Rush et al., 2012; Podlaska et al., 2012). Samples for this investigation were collected from aboard the R/V *Knorr* in December 2008–January 2009 from 13°N 105°W (Station 1, "Tehuantepec Bowl"; 3235 m total depth) and 9°N 90°W (Station 8, "Costa Rica Dome"; 3525 m total depth; Fig. 1).

2.1. In situ filtration.

Seawater was sequentially filtered in situ via submersible pumps (WTS-LV 08 upright: McLane Research Laboratories, Inc.), with total collected volumes of 200–1890 L per depth. Six to seven depths were sampled at each station, targeting the surface; upper and lower fluorescence maxima; upper oxycline; upper, middle, and lower OMZ; and lower oxycline, as defined by a Seabird CTD package (Fig. 2). Most pumps were equipped with three filter tiers, each 142-mm in diameter. The first tier was fitted with an acid-cleaned 53 μm-mesh Nitex screen, the second with one or two (stacked) glass fiber filters (GF/F; 0.7 μm pore-size), and the last with a polyethersulfone filter (Pall Supor; 0.2 μm pore-size). Overall lipid yields for X-POM versus L-POM were similar regardless of the use of one (Station 1) or two (Station 8) GF/Fs on the middle tier, suggesting that filters retained structural integrity and separated particle size classes roughly uniformly across samples. For several depths at Station 1, pumps were equipped with only two filter tiers, and only Nitex and GF/F filters were used. Average flow rates were 2.1–3.6 L min^{-1} when Supor filters were used and 5.3–7.0 L min^{-1} when Supor filters were not used. Each filter was wetted with sterile-filtered deionized water before tiers were assembled for deployment. Pumps equilibrated with water at the sampling depths for 20–30 min before pumping commenced. Upon recovery, pumps were activated briefly to remove excess

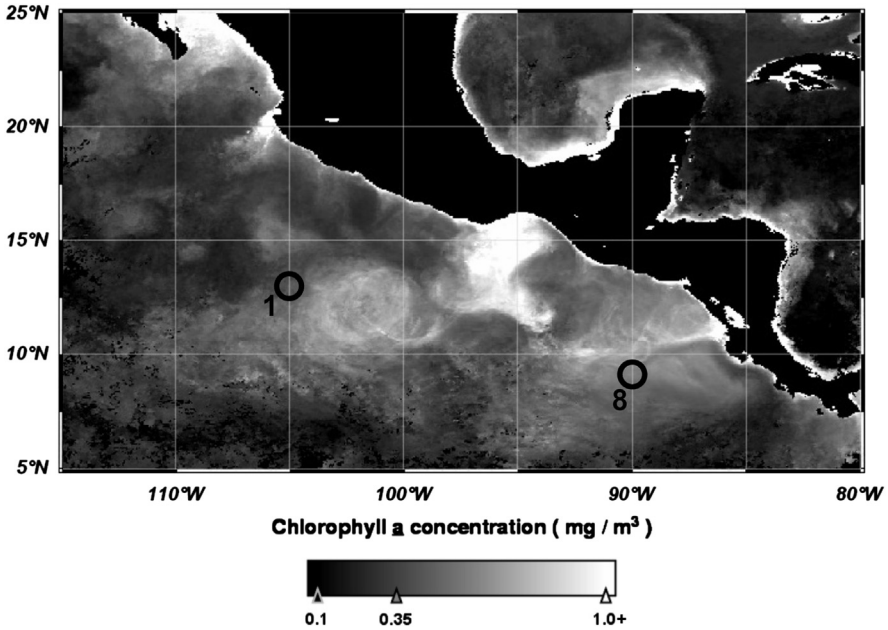

Fig. 1. Study sites in the Eastern Tropical North Pacific: Station 1, 13°N 105°W; Station 8, 9°N 90°W, and mean chlorophyll-*a* concentration from remote sensing by Aqua MODIS (Moderate-resolution Imaging Spectroradiometer) between 10 Dec 2008 and 10 Jan 2009 (Feldman and McClain, accessed 2013; edited in SeaDAS).

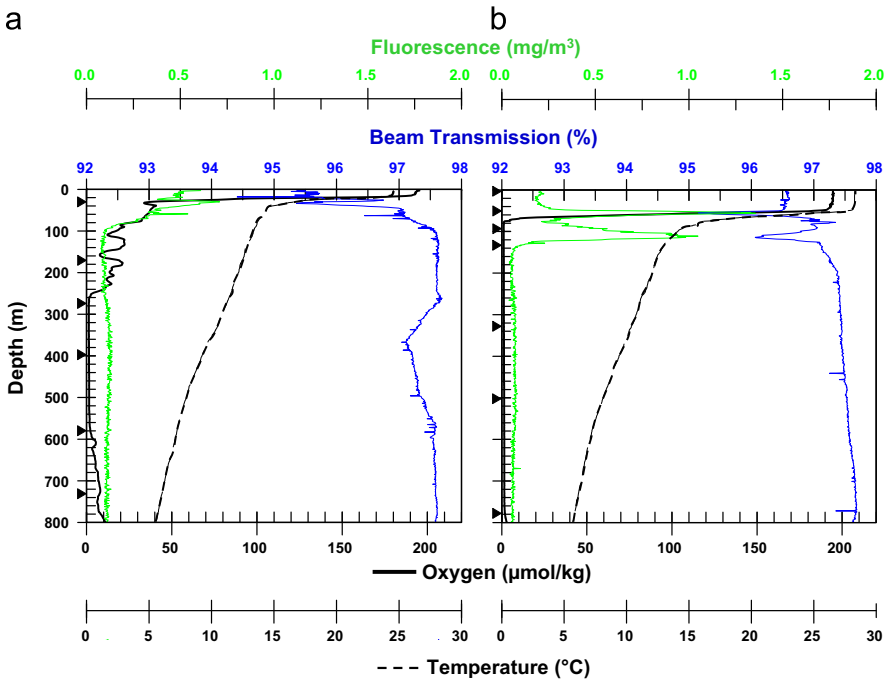

Fig. 2. Water column properties in the ETNP: (a) Station 8 (9°N, 90°W); (b) Station 1 (13°N, 105°W). Fluorescence (solid green), beam transmission (solid blue), temperature (dashed black), and dissolved oxygen concentrations (thick black) are shown for the upper 800 m of each water column. Sampling depths are indicated with black triangles. (For interpretation of the references to color in this figure legend, the reader is referred to the web version of this article.)

seawater from filters. Filters were removed using clean forceps and frozen immediately at −70 °C.

2.2. Extraction and separation of polar lipid fractions

GF/F and Supor filters were cut into wedges and extracted using physical disruption (freeze-thaw and bead-beating), detergent extraction (1:1 B-PER and Y-PER, Pierce), and phenol/chloroform extraction (Trizol LS, Invitrogen). Nitex filters (> 53 μm particles) were not analyzed here. The detergent suspension was separated from filter material by centrifugation before adding phenol and chlorinated solvents, thereby preventing the dissolution of polymer filter material into the extract. After phase separation, the aqueous phase containing nucleic acids was removed for later analysis. Proteins were precipitated from the remaining organic phase using cold isopropanol and pelletized by centrifugation. The supernatant organic phase, containing lipids, was removed and washed successively against weak NaOH and H_2O. This approach is known as CEP (Comprehensive Extraction Protocol). The relative yield of IPL classes varied in a test of CEP versus the Bligh and Dyer (1959) method: glycolipid yield was higher using Bligh and Dyer, while phospholipid yield was higher using CEP (Close, 2012). Variation in yield is common across lipid extraction methods (Huguet et al., 2010). Accordingly, we consider the absolute concentration results (Tables 1 and 2) to be approximate, but relative patterns in these values should be internally consistent across all samples.

The total lipid extract (TLE) was dried (N_2, < 40 °C) and separated on 100–200 mesh, 60 Å, pre-combusted SiO_2 gel. Nonpolar lipids were eluted in 75% hexane/25% ethyl acetate (v/v); glycolipids in 75% ethyl acetate/25% methanol (v/v); and phospholipids in 100% methanol. Separation of the glycolipid fraction was optimized using intact glycolipid and phospholipid standards (1,2-dihexadecanoyl-3-*O*-(α-D-glucopyranosyl)-*sn*-glycerol, 1,2-diheptadecanoyl-*sn*-glycero-3-phosphoethanolamine, and 1,2-ditricosanoyl-*sn*-glycero-3-phosphocholine; Avanti Polar Lipids, Inc., Alabaster, AL); our elution scheme is more polar than the analogous glycolipid fraction of Pitcher et al. (2009). Coarse separation of glycolipid and phospholipid fractions was confirmed by headgroup analysis via HPLC-QToF on an individual sample (Sturt et al., 2004; Schubotz et al., 2011a, 2011b). Glycosidic head groups were overwhelmingly abundant in the "glycolipid" fraction, with a smaller number of phosphatidylglycerol peaks also detected. Similarly, diverse and abundant phosphatic head groups were present in the "phospholipid" fraction, along with a small fraction of glycosidic head groups. Betaine head groups partitioned into the phospholipid fraction, while sulfolipids were found in the glycolipid fraction. More specific quantitation of IPL head groups was not attempted here and is not straightforward, even with reference standards, since response factors vary greatly using HPLC methods (Schubotz et al., 2009, 2011a, 2011b). Aliquots of polar lipid fractions from selected samples were derivatized to trimethylsilyl (TMS) ethers before saponification and were found (by GC–MS) to contain no free fatty acids.

2.3. Isotope analysis of FAMEs.

Polar lipid fractions were saponified (0.5 N KOH in methanol, 100 °C, 2 h). Neutral lipids were extracted from the basic mixture, which was then acidified (HCl, pH ~2) before extraction of fatty acids (90% hexane/10% dichloromethane, v/v). Fatty acids were converted to fatty acid methyl esters (FAMEs) by heating in 10% BF_3 in methanol (70 °C, 20 min). Nanopure water was added to stop the reaction, and FAMEs were extracted from the reaction mixture with hexane. Fatty acid standards of known ^{13}C content were identically methylated to determine the ^{13}C content of the derivative carbon.

FAMEs were identified by gas chromatography–mass spectrometry (GC–MS; Agilent 6890N GC, 5973 MS) equipped with a 30 m HP-5MS column. Absolute abundance of the natural $C_{16:0}$ FAME in each sample was determined by comparison of the peak area with a $C_{19:0}$ FAME standard added at known concentration.

Natural ^{13}C content of individual FAMEs was determined by gas chromatography – isotope ratio monitoring mass spectrometry using a 30 m DB-5MS column (GC-IRMS: Thermo Scientific Trace

Table 1
$\delta^{13}C$ values, error in $\delta^{13}C$ values, and concentration of individual fatty acids collected from polar lipid classes at Station 8. Weighted average $\delta^{13}C$ values ($\delta^{13}C_{avg}$) are shown for each depth and size/polarity fraction. Fatty acid notation is (Carbon chain length):(Number of double bonds). Known isomers of $C_{18:1}$ are identified in ω-notation. Isomers of unknown double-bond position are identified as a-, b-, c-, etc., and this notation refers to the same compounds across samples.

	L (0.7–53 μm) Glyco			X (0.2–0.7 μm) Glyco			L (0.7–53 μm) Phospho			X (0.2–0.7 μm) Phospho		
	$\delta^{13}C$ (‰)	σ	ng/L	$\delta^{13}C$ (‰)	σ	ng/L	$\delta^{13}C$ (‰)	σ	ng/L	$\delta^{13}C$ (‰)	σ	ng/L
30 m												
12:0	−28.1	0.7	0.6	−27.7	0.9	1.0	–	–	0.4	–	–	0.3
14:0	−29.5	1.0	15.8	−29.9	1.0	18.5	−29.4	0.9	5.3	−28.8	0.6	4.1
14:1	−30.9	0.6	1.1	−30.9	0.6	1.4	–	–	0.3	–	–	–
15:0	−29.1	0.7	0.6	–	–	0.4	–	–	1.0	–	–	0.4
i-15:0	−27.4	1.0	0.5	−25.6	1.0	0.8	–	–	0.8	–	–	0.4
16:0	−28.8	1.0	45.4	−28.9	1.0	21.3	−28.7	0.8	13.6	−27.6	0.6	20.1
16:1	–	–	0.8	−30.1	1.0	0.7	–	–	–	–	–	3.6
16:1-c	–	–	–	–	–	0.7	−29.0	1.0	2.0	–	–	–
16:1+16:2	−31.0	0.8	10.8	−30.9	0.9	14.6	−31.8	1.0	4.0	−24.7	0.5	3.3
16:4	−33.2	0.5	1.3	–	–	–	–	–	–	–	–	–
17:0	−27.4	1.0	0.4	–	–	0.2	–	–	–	–	–	–
17:1	–	–	0.1	−23.8	1.0	1.1	–	–	0.8	–	–	0.7
18:0	−28.6	1.0	15.8	−28.5	1.0	8.9	−29.2	0.5	5.2	−26.7	0.5	22.8
18:1ω7	−27.7	0.5	1.7	−25.9	0.5	3.2	−28.3	0.5	1.4	−27.2	1.0	3.0
18:1ω9	−31.0	0.5	3.1	−30.3	0.5	2.2	−34.0	1.0	1.6	–	–	1.4
18:2	−32.2	0.5	1.2	−32.3	1.0	0.8	−34.9	1.0	0.9	–	–	1.0
18:4	−34.9	0.9	3.8	−34.5	1.0	1.2	−34.4	0.5	1.4	–	–	1.0
18:4-b	−30.6	1.3	2.0	−29.2	1.0	0.7	–	–	0.7	–	–	–
20:5	−27.0	0.4	1.3	−28.4	1.0	0.9	−29.2	0.7	1.4	–	–	0.8
22:6	−27.8	0.5	3.4	−30.5	4.5	1.8	−32.9	1.0	3.6	−31.5	1.0	2.3
Other	–	–	2.4	–	–	0.4	–	–	–	–	–	–
Avg or sum	**−29.4**	**0.5**	**112.0**	**−29.5**	**0.4**	**80.6**	**−30.1**	**0.3**	**44.4**	**−27.3**	**0.3**	**65.2**
170 m												
12:0	−27.4	0.8	0.3	−27.3	0.7	0.2	–	–	0.02	–	–	0.6
14:0	−29.4	1.0	0.7	−29.5	1.0	0.7	–	–	0.1	−29.7	0.6	1.9
16:0	−28.5	1.0	2.5	−26.6	1.0	0.8	−28.0	0.9	0.6	−26.7	0.7	3.9
16:1	–	–	0.1	−24.8	1.0	0.1	–	–	0.04	−24.5	1.0	0.5
16:1+16:2	–	–	–	–	–	–	−26.7	1.0	0.2	–	–	–
18:0	−28.4	1.0	1.9	−27.2	1.0	1.0	−29.4	0.5	0.6	−27.5	0.6	5.4
18:1ω7	–	–	0.1	–	–	0.1	–	–	–	–	–	0.2
18:1ω9	−26.5	1.0	0.2	–	–	0.05	–	–	–	–	–	–
22:6	−30.6	1.0	0.2	–	–	0.03	–	–	0.1	–	–	–
Other	–	–	0.1	–	–	0.1	–	–	0.3	–	–	0.1
Avg or sum	**−28.5**	**0.6**	**5.9**	**−27.5**	**0.5**	**3.1**	**−28.5**	**0.4**	**1.9**	**−27.4**	**0.4**	**12.6**
274 m								[a]				
12:0	−27.5	0.8	0.3	−27.6	0.7	0.2	–	–	–	–	–	0.03
14:0	−29.1	1.0	0.7	−29.3	1.0	1.1	–	–	0.1	–	–	0.1
16:0	−27.6	1.0	1.5	−27.0	1.0	0.7	−27.3	0.6	1.2	−27.1	0.9	1.6
16:1	–	–	0.1	−21.1	0.8	0.2	–	–	0.1	−27.0	0.6	0.4
18:0	−27.7	1.0	1.2	−27.8	1.0	0.7	−29.0	0.8	1.3	−27.2	0.6	2.5
18:1ω9	−27.3	0.6	0.5	–	–	0.1	–	–	–	–	–	–
22:1	−32.0	1.4	0.3	–	–	0.2	–	–	–	–	–	–
22:6	−24.9	1.0	0.1	–	–	0.1	–	–	–	–	–	–
Other	–	–	0.4	–	–	0.2	–	–	0.2	–	–	0.3
Avg or sum	**−28.0**	**0.4**	**5.1**	**−27.7**	**0.5**	**3.4**	**−28.2**	**0.5**	**2.9**	**−27.2**	**0.4**	**5.0**

398 m									[a]			[a]
12:0	−27.9	1.0	0.3	−27.5	0.7	1.1	–	–	0.1	–	–	–
14:0	−28.6	1.0	1.0	−28.9	1.0	2.8	−25.1	1.0	0.3	–	–	0.2
16:0	−26.0	1.0	2.2	−27.6	1.0	4.2	−26.1	0.6	1.8	−27.0	0.7	2.6
16:1	−26.3	1.0	0.3	–	–	0.4	−27.0	1.2	0.7	−27.3	4.1	0.6
17:1	–	–	0.1	–	–	–	−23.9	0.7	0.5	–	–	0.3
18:0	−27.6	1.0	1.0	−27.5	1.0	2.7	−28.5	0.5	1.5	−27.4	0.7	3.3
18:1ω7	−28.0	1.0	0.4	−27.4	1.0	0.7	−29.3	0.5	0.6	–	–	0.3
18:1ω9	–	–	0.2	−26.9	0.5	1.5	–	–	0.1	–	–	–
22:6	−23.6	0.6	0.7	–	–	0.1	−22.9	0.4	0.6	–	–	–
Other	–	–	1.2	–	–	1.1	–	–	0.8	–	–	–
Avg or sum	**−26.6**	**0.4**	**7.4**	**−27.8**	**0.4**	**14.6**	**−26.6**	**0.3**	**6.9**	**−27.2**	**0.5**	**7.3**
580 m												[a]
12:0	−27.6	0.9	0.3	−27.7	0.8	0.5	–	–	–	–	–	–
14:0	−29.7	1.0	0.7	−29.7	1.0	1.3	–	–	0.1	–	–	0.03
16:0	−27.4	1.0	0.8	−28.1	1.1	1.2	−27.3	0.8	0.4	−26.9	0.7	0.2
16:1	–	–	–	–	–	0.2	–	–	0.1	−26.6	0.9	0.1
18:0	−27.9	1.0	1.1	−28.2	1.0	1.3	−28.4	0.5	0.6	−28.4	0.5	0.2
18:1ω9	–	–	–	−27.6	0.7	0.4	–	–	–	–	–	–
Other	–	–	0.3	–	–	0.3	–	–	0.1	–	–	0.1
Avg or sum	**−28.1**	**0.5**	**3.2**	**−28.5**	**0.5**	**5.3**	**−27.9**	**0.4**	**1.3**	**−27.5**	**0.4**	**0.6**
730 m			[a]									
12:0	−28.5	1.0	0.2	−27.7	0.9	0.3	–	–	0.01	–	–	–
14:0	−29.8	1.0	0.5	−29.8	1.1	1.3	−25.2	1.0	0.1	–	–	0.04
16:0	−27.4	1.0	0.5	−28.8	1.0	1.4	−27.1	0.6	0.3	−27.3	0.7	0.4
16:1	–	–	0.1	–	–	0.1	−29.1	1.0	0.1	−23.4	0.8	0.1
18:0	–	–	0.00	−28.3	1.0	0.9	−28.8	0.5	0.4	−28.2	0.5	0.5
18:1ω9	–	–	0.1	−26.5	1.0	0.2	–	–	–	–	–	–
22:1	–	–	0.1	−31.3	0.8	0.3	–	–	–	–	–	–
OH-20:0	–	–	–	−30.0	0.6	0.7	–	–	–	–	–	–
Other	–	–	0.2	–	–	0.2	–	–	0.1	–	–	–
Avg or sum	**−28.6**	**0.5**	**1.6**	**−29.1**	**0.4**	**5.4**	**−28.1**	**0.3**	**0.9**	**−27.2**	**0.4**	**1.1**

Unspecified isomers distinguished as -a, -b, -c, etc.
Italics = unconfirmed structure.

[a] Estimated after loss.

Table 2
$\delta^{13}C$ values, error in $\delta^{13}C$ values, and concentration of individual fatty acids collected from polar lipid classes at Station 1. Weighted average $\delta^{13}C$ values ($\delta^{13}C_{avg}$) are shown for each depth and size/polarity fraction. Fatty acid notation is (Carbon chain length):(Number of double bonds). Known isomers of $C_{18:1}$ are identified in ω-notation. Isomers of unknown double-bond position are identified as a-, b-, c-, etc., and this notation refers to the same compounds across samples.

	L (0.7–53 μm) Glyco			X (0.2–0.7 μm) Glyco			L (0.7–53 μm) Phospho			X (0.2–0.7 μm) Phospho		
	$\delta^{13}C$ (‰)	σ	ng/L	$\delta^{13}C$ (‰)	σ	ng/L	$\delta^{13}C$ (‰)	σ	ng/L	$\delta^{13}C$ (‰)	σ	ng/L
3 m												
12:0	−27.9	0.8	0.4	*Not collected*			–	–	0.2	*Not collected*		
14:0	−29.0	1.0	11.8				−27.5	0.6	1.6			
14:1	−29.0	0.7	1.0				–	–	0.1			
16:0	−27.4	1.0	10.5				−26.7	0.6	3.4			
16:1	–	–	–				−25.9	0.5	1.0			
16:1 − b	−29.2	0.7	5.8				–	–	–			
18:0	−27.9	1.0	2.4				−28.9	1.4	1.9			
18:1ω7	−23.1	0.8	0.6				−24.1	0.4	0.8			
18:1ω9	−27.1	0.7	1.2				–	–	0.5			
18:2	−28.1	0.8	0.4				–	–	0.2			
18:4	−27.5	0.9	0.5				–	–	–			
22:6	−25.1	0.5	0.8				−26.2	0.4	0.5			
Other	–	–	1.5				–	–	0.8			
Avg or sum	**−28.2**	**0.5**	**36.9**				**−26.9**	**0.3**	**10.9**			
52 m												
12:0	−28.4	0.8	1.6	*Not collected*			–	–	0.2	*Not collected*		
14:0	−30.8	1.0	31.4				−29.4	0.7	2.0			
14:1	−32.8	0.7	3.2				–	–	0.1			
15:0	−29.6	0.6	1.1				–	–	0.2			
i-15:0	−25.8	0.6	0.7				−23.7	0.6	0.3			
16:0	−29.0	1.0	24.3				−29.0	0.6	4.0			
16:1	−29.0	0.6	1.9				−28.9	0.6	1.6			
16:1 + 16:2	−32.1	0.8	23.3				–	–	0.3			
16:2	–	–	–				−37.2	0.6	0.4			
16:3	−32.7	0.6	1.4				–	–	–			
16:4	−33.8	0.8	4.6				−35.2	1.0	0.4			
18:0	−28.6	1.5	5.9				−28.1	0.5	1.7			
18:1ω7	−26.8	0.8	2.7				−27.0	0.5	1.1			
18:1ω9	–	–	–				−32.1	0.5	1.0			
18:1 + 18:3	−31.4	0.7	7.1				–	–	–			
18:2	−33.9	0.8	3.4				−36.9	0.5	0.6			
18:3	−32.0	0.7	5.7				–	–	0.3			
18:3 + 18:4	−34.3	0.5	23.2				–	–	–			
18:4	−34.7	0.5	18.7				−36.4	0.5	0.6			
20:5	−27.6	0.5	3.9				−29.7	0.6	0.9			
22:6	−27.9	0.5	6.8				−28.9	1.1	2.4			
Other	–	–	7.1				–	–	1.8			
Avg or sum	**−31.5**	**0.3**	**177.9**				**−29.8**	**0.2**	**19.8**			
91 m												
12:0	−27.7	0.8	0.6	*Not collected*			−26.9	1.0	0.3	*Not collected*		
14:0	−28.5	1.0	13.3				−26.6	0.7	5.7			
br-14:0	–	–	–				−26.0	1.0	0.4			
14:1	−29.5	0.7	4.0				−22.0	0.9	0.7			
15:0	−28.5	0.8	0.8				−28.6	0.9	0.9			
i-15:0	−25.0	0.7	0.6				−24.6	0.8	0.9			
a-15:0	−24.7	0.7	0.5				−25.2	0.7	1.0			

16:0	−27.9	1.0	8.2				−27.5	0.6	10.2			
16:1	−29.5	1.0	16.2				−26.2	0.9	12.8			
16:1-b	−28.1	1.0	0.8				−25.2	1.0	2.4			
16:1-c	−23.8	1.0	0.9				−25.2	0.5	1.2			
16:2	−29.3	1.0	0.7				–	–	–			
17:0	−26.3	1.0	0.8				−25.8	1.0	0.3			
18:0	−26.5	1.0	0.7				−27.9	0.7	1.0			
18:1ω7	−26.9	0.8	1.2				−25.5	0.5	3.8			
18:1ω9	−29.5	0.8	1.1				−28.6	0.6	2.0			
18:2	–	–	0.4				−33.2	1.0	0.6			
18:4	−33.5	0.7	0.7				–	–	0.3			
20:5	−28.8	1.1	1.0				−28.5	0.6	2.1			
22:6	−27.8	0.6	2.2				−27.3	1.1	4.7			
22:6-c	–	–	0.4				−27.6	1.5	0.9			
Other	–	–	1.2				–	–	3.1			
Avg or sum	**−28.6**	**0.4**	**56.3**				**−26.7**	**0.3**	**55.2**			
128 m												
12:0	−27.9	0.9	0.9	−27.7	0.8	0.6	–	–	0.1	–	–	0.1
14:0	−30.9	1.0	5.6	−29.7	1.0	5.6	−26.5	1.0	0.5	−24.5	0.6	1.2
14:1	−33.1	1.0	0.7	−29.0	1.0	0.5	–	–	0.1	–	–	0.2
15:0	−29.4	1.0	0.4	–	–	0.4	–	–	0.1	−24.7	1.0	0.3
i-15:0	−24.6	1.0	0.3	−22.1	0.7	0.6	−21.9	1.0	0.2	−22.0	1.1	0.6
a-15:0	−24.5	1.0	0.2	−25.7	0.7	0.4	−22.7	1.0	0.2	−22.3	1.3	0.4
unk-15:0	–	–	–	–	–	–	–	–	–	−43.8	1.0	0.3
16:0	−27.5	1.1	6.6	−25.7	1.0	5.8	−27.0	1.0	1.7	−25.2	0.7	5.2
16:1	−32.3	0.6	3.5	–	–	5.0	−23.4	1.0	0.8	−22.9	0.7	5.4
16:1−c	−29.9	1.0	0.5	–	–	0.6	–	–	0.1	−22.2	0.5	0.7
br-17:0	–	–	–	–	–	–	–	–	0.1	−31.7	1.0	0.3
17:1	–	–	–	–	–	–	−25.0	1.0	0.6	–	–	0.3
18:0	−26.9	1.0	2.8	−27.0	1.0	1.7	−28.9	0.6	1.2	−27.9	0.5	1.4
18:1ω7	−29.4	1.0	0.7	−23.2	1.2	1.9	−24.5	1.0	0.4	−22.2	0.6	2.7
18:1−c	−27.8	1.0	0.8	–	–	–	–	–	–	–	–	–
20:5	−32.1	1.0	0.5	–	–	0.4	–	–	0.1	−24.0	0.7	0.6
22:1	−35.1	1.0	0.4	−30.2	1.0	0.6	–	–	–	–	–	–
22:6	−26.7	0.9	1.1	–	–	0.5	−27.4	1.0	0.2	−26.9	0.4	0.4
Other	–	–	0.3	–	–	2.3	–	–	0.4	–	–	1.5
Avg or sum	**−29.3**	**0.4**	**25.2**	**−27.0**	**0.4**	**26.7**	**−26.2**	**0.3**	**6.7**	**−24.2**	**0.3**	**21.6**
326 m												
12:0	−27.8	0.7	0.6	−27.8	0.7	0.7	–	–	0.05	–	–	0.03
14:0	−30.2	1.0	1.7	−30.0	1.0	3.0	−24.8	1.0	0.2	−25.2	0.6	0.4
15:0	–	–	0.2	–	–	0.1	–	–	0.1	−22.9	1.0	0.1
i-15:0	–	–	0.1	–	–	0.2	–	–	0.1	−21.3	1.7	0.2
a-15:0	–	–	0.1	–	–	0.1	−20.8	1.0	0.2	−20.3	1.5	0.2
unk-15:0	–	–	–	–	–	–	–	–	–	−41.9	1.0	0.2
unk-15:0-*c*	–	–	–	–	–	–	–	–	–	−38.9	1.0	0.1
16:0	−27.1	1.0	3.5	−25.1	1.0	4.5	−26.0	0.6	1.1	−24.9	1.7	2.9
16:1	−27.0	1.0	0.4	−22.6	0.5	0.9	−27.0	0.6	0.9	−22.4	0.8	2.5
16:1-c	–	–	0.2	–	–	0.2	–	–	0.2	−22.4	1.0	0.3
br-17:0	–	–	–	–	–	–	–	–	0.1	−26.4	0.5	0.5
17:1	–	–	–	–	–	–	−23.1	1.0	0.3	−26.3	5.3	0.4
18:0	−27.0	1.0	2.3	−24.7	1.0	4.3	−26.7	0.6	0.5	−27.3	0.7	0.5
18:1ω7	–	–	0.5	−24.7	1.0	0.7	−28.8	0.5	0.6	−22.7	0.6	1.6
18:1ω9	−26.2	0.5	0.6	–	–	–	–	–	–	−26.3	0.8	1.0
20:5	–	–	0.1	–	–	0.3	–	–	0.1	−23.5	1.3	0.2
22:1	−32.8	0.8	0.4	−34.2	1.0	0.4	–	–	–	–	–	–
22:6	−25.8	0.5	0.5	–	–	0.2	−25.3	1.0	0.2	−27.4	1.0	0.2
Other	–	–	0.7	–	–	–	–	–	0.2	–	–	0.7

Table 2 (*continued*)

	L (0.7–53 μm) Glyco			X (0.2–0.7 μm) Glyco			L (0.7–53 μm) Phospho			X (0.2–0.7 μm) Phospho		
	$\delta^{13}C$ (‰)	σ	ng/L	$\delta^{13}C$ (‰)	σ	ng/L	$\delta^{13}C$ (‰)	σ	ng/L	$\delta^{13}C$ (‰)	σ	ng/L
Avg or sum	**−27.7**	**0.4**	**11.9**	**−26.2**	**0.4**	**15.6**	**−26.3**	**0.2**	**5.0**	**−24.5**	**0.5**	**11.9**
502 m												
12:0	−27.8	0.7	0.2	*Not collected*			–	–	0.04	*Not collected*		
14:0	−29.4	1.0	0.9				−25.1	1.0	0.2			
a-15:0	–	–	0.1				−21.8	1.0	0.1			
16:0	−27.6	1.0	2.6				−26.6	0.9	1.0			
16:1	−27.4	0.5	0.4				−25.7	0.7	0.6			
17:0	−26.9	1.0	0.3				–	–	–			
18:0	−27.2	1.0	1.4				−27.7	0.5	0.8			
18:1ω7	−28.5	0.7	0.4				−29.5	0.5	0.4			
18:1ω9	−27.0	0.5	0.3				–	–	0.2			
22:1	−32.5	1.5	0.9				–	–	–			
22:6	−25.2	0.7	0.3				–	–	0.1			
Other	–	–	0.6				–	–	0.4			
Avg or sum	**−28.2**	**0.4**	**8.6**				**−26.8**	**0.3**	**3.7**			
778 m			[a]									
16:0	−28.8	1.0	8.0	*Not collected*			*Sample lost*			*Not collected*		
18:0	−28.2	1.0	11.2									
Other	–	–	5.2									
Avg or sum	**−28.5**	**0.7**	**24.4**									

Unspecified isomers distinguished as -a, -b, -c, etc.
Italics = unconfirmed structure.

[a] Estimated after loss.

GC Isolink-Conflo IV-Delta V Advantage). Each sample was measured 3–6 times at varying concentrations in order to resolve FAME peaks of varying sizes. IRMS peak areas were used to determine the concentration of each compound relative to $C_{16:0}$ FAME. Mean $\delta^{13}C$ values were determined from replicate runs, and only peaks of amplitude > 0.4 V (m/z 44) were accepted. The contribution of the methyl carbon from BF_3/MeOH was removed by isotope mass balance. Error in $\delta^{13}C$ values is reported as $\pm 1\sigma$ replicate error propagated with $\pm 1\sigma$ error in the value for the added methyl carbon (Tables 1 and 2). The $\delta^{13}C$ value of the methyl carbon was determined separately via > 40 replicate runs of FAME standards. Absolute instrument performance was checked regularly using the external B3 alkanes reference material, while internal run performance was checked via co-injected C_{32} n-alkane (http://mypage.iu.edu/~aschimme/n-Alkanes.html). Errors are reported as $\pm 1‰$ for any compound that was measured only once above the 0.4 V threshold. All values were corrected for instrument drift (over time in individual runs) and linearity (instrument average).

Minor contributions of $C_{14:0}$, $C_{16:0}$, and $C_{18:0}$ from unidentified acyl-containing contaminants in the extraction detergent were found in the glycolipid fraction only. Relative proportions and $\delta^{13}C$ values of these compounds were measured in blanks using the same methods as for samples. Absolute concentrations were determined by assuming that the blank contributed 100% of the $C_{18:0}$ in the sample with the lowest glycolipid content (Station 8, 730 m: 370 ng or 0.6 ng L^{-1} $C_{18:0}$) and scaling the contribution of exogenous $C_{14:0}$ and $C_{16:0}$ proportionally. The appropriate concentrations of detergent-derived compounds were subtracted from glycolipid results by adjusting for the volume of detergent used in each sample extraction (mean $3 \pm 3\%$, $11 \pm 7\%$, and $29 \pm 12\%$ corrections to $C_{14:0}$, $C_{16:0}$, and $C_{18:0}$ sample concentrations, respectively), and the $\delta^{13}C$ values for these compounds were corrected by isotope mass balance (mean $0.0 \pm 0.0‰$, $0.2 \pm 0.3‰$, and $0.3 \pm 0.2‰$ corrections, respectively). Errors are reported as $\pm 1‰$ for compounds to which this correction was applied.

2.4. Analysis of bulk POM

Organic carbon (%OC), total nitrogen (%TN) and ^{13}C content of bulk 0.7–53 μm POM were determined on GF/Fs from companion pump deployments at the same locations and depths. Plugs (14 mm diameter) were removed from each GF/F with a cork borer, each plug representing 3.3% of the filter. Filter plugs were exposed with fuming HCl for 48 h and dried at 40 °C. Samples were analyzed with a Thermo Scientific Flash EA Series 1112 coupled with a Finnigan Conflo IV interfaced to a Thermo Delta V isotope ratio mass spectrometer. Instrument calibration was against an internal laboratory chitin powder standard and USGS 40 and 41 international isotope standards (Qi et al., 2003).

3. Results

3.1. Oceanographic setting

Water column properties were described previously by Wishner et al. (2013) and are similar to those reported for the previous year (Rush et al., 2012; Podlaska et al., 2012). Briefly, Station 8 is characterized by a shallow mixed layer (~10 m) and a sharp drop in oxygen concentration (40 μmol kg^{-1} at 40 m). Below this, oxygen concentrations are suboxic (10–30 μmol kg^{-1}) – with variability caused by advection of oxygenated waters (Lewitus and Broenkow, 1985) – until dropping to < 2 μmol kg^{-1} at ~275 m and remaining < 1.5 μmol kg^{-1} between 350 m and 550 m (Fig. 2a). In the mid-OMZ an increase in particle concentration is apparent from a broad decrease in beam transmission (660 nm, Fig. 2a). The primary chlorophyll maximum is centered around 30 m, and a poorly-defined lower chlorophyll maximum at Station 8 is only sometimes evident in fluorescence profiles. At Station 1 the mixed layer is deeper (~50 m) and oxygen concentration drops abruptly from ~200 μmol kg^{-1} in the mixed layer to < 3 μmol kg^{-1} at 80 m (Fig. 2b). An upper chlorophyll maximum (centered around 52 m) and a lower chlorophyll maximum (centered around 90–120 m, within the OMZ) are both prominent. Oxygen concentrations remained < 2 μmol kg^{-1} between about 110 m and 760 m before rising beneath this depth.

3.2. Absolute abundance of fatty acids

Station 8: In the photic zone, extra-small particulate material (X-POM, 0.2–0.7 μm) contains approximately as much total IPL as the larger (L-POM, 0.7–53 μm) size class (~150 ng L^{-1}; Table 1 and Fig. 3a and b). In X-POM, IPLs are evenly divided between glycolipids and phospholipids, while in L-POM the glycolipids are over two-fold more abundant than phospholipids. IPL-fatty acid concentrations in upper subphotic waters (170 m) drop to 3–17%

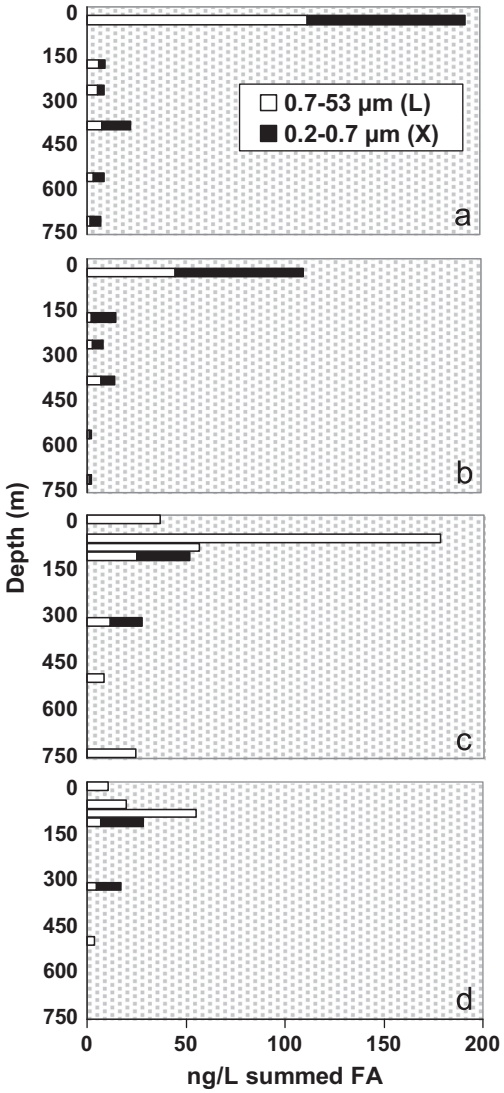

Fig. 3. Approximate concentrations of summed fatty acids by depth and size fraction, in ng L^{-1}: 0.7–53 μm (L-POM, white) and 0.2–0.7 μm (X-POM, black). (a) Station 8 glycolipids; (b) Station 8 phospholipids; (c) Station 1 glycolipids; and (d) Station 1 phospholipids.

of the concentrations in the chlorophyll maximum (Fig. 3a and b). At 170 m, the majority of IPLs are in X-POM, and most are phospholipids. The mid-OMZ (398 m) is marked by a relative increase in lipid concentrations compared to adjacent sampling depths, most prominently in glycolipids and particularly in X-POM. This increase marks a shift in the size distribution of glycolipids; below 300 m, X-POM contains > 50% of the glycolipids, whereas in the photic zone and the upper OMZ (170, 274 m) L-POM contains > 50% of the glycolipids. A smaller increase in the concentration of phospholipids occurs at 398 m, mostly within L-POM. The overall increase in IPL abundance in the mid-OMZ is accompanied by a broad peak in beam attenuation (Fig. 2a) and total particulate organic carbon (POC) concentrations (Table 3) and corresponds to previous observations of mid-OMZ peaks in pigment concentrations (Lewitus and Broenkow, 1985), prokaryotic cell counts, and nitrite concentration (Podlaska et al., 2012) in the Costa Rica Dome.

Station 1: In the photic zone at Station 1, L-POM contains a higher abundance of IPL-fatty acids than at Station 8; X-POM was only collected at subphotic depths. The highest concentration of total IPL coincides with the upper chlorophyll maximum (198 ng L^{-1}; 52 m; ~190 μmol kg^{-1} O_2, fully oxic). However, concentrations of phospholipids are highest at the lower chlorophyll maximum, within the upper OMZ (55 ng L^{-1}; 91 m; < 3 μmol kg^{-1} O_2). The glycolipid abundance exceeds the phospholipid abundance at all other depths, by a factor as large as 9:1 at 52 m. Below the lower chlorophyll maximum IPL concentrations in L-POM quickly decrease to ~25% of maximum concentrations seen at 52 m. Where X-POM was sampled (128 and 326 m) it contains a higher IPL concentration than L-POM, and the X:L ratio is greater in the phospholipid fraction than it is in the glycolipid fraction. Although samples collected the previous year at Station 1 displayed a mid-OMZ peak in POC concentration similar to that at Station 8 (Wakeham, unpublished data), no such peak was evident in our Station 1 lipids, POC, or beam attenuation. However, our sampling resolution may have been insufficient to detect such a feature.

3.3. Distributions of individual fatty acids

3.3.1. Patterns with depth

Fatty acids from all polarity fractions and size classes are dominated by straight-chain saturated compounds, *n*-$C_{12:0}$–$C_{18:0}$ at all depths (Station 8: 52–93% of total compounds, Station 1: 33–81%; Tables 1 and 2). The upper chlorophyll maximum at both stations contains high proportions of unsaturated compounds (Fig. 4), most concentrated in L-POM glycolipids at Station 1 (61% unsaturated) and in L-POM phospholipids at Station 8 (41% unsaturated), with multiple positional isomers of $C_{22:6}$, $C_{20:5}$, $C_{18:4}$, $C_{18:3}$, $C_{18:2}$, $C_{18:1}$, $C_{16:2}$, and $C_{16:1}$, and single identifiable isomers of $C_{16:4}$, $C_{17:1}$, and $C_{14:1}$. This distribution is characteristic of mixed marine phytoplankton assemblages (Harwood and Russell, 1984; Wakeham, 1995).

The proportion of straight-chain, saturated compounds generally is lowest at the chlorophyll maximum and increases below the photic zone. However, the mid-OMZ at both stations contained a higher relative proportion of unsaturated compounds than at adjacent depths (glycolipids and phospholipids, Station 8; phospholipids only, Station 1).

Table 3
$\delta^{13}C$ values, organic carbon concentration, and molar organic *C*/*N* ratios measured from bulk L-POM, both stations. Error in $\delta^{13}C$ values is ± 0.1‰.

Depth (m)	$\delta^{13}C$ (‰)	μgC/L	*C*/*N*
Station 8:			
28*	−21.4	19.6	6.0
156	−20.4	3.7	7.0
264	−20.9	2.8	6.0
409	−20.5	5.5	7.2
540	−23.1	3.9	6.5
690	−23.2	2.9	8.6
Station 1:			
3	−21.1	13.4	8.4
52*	−24.0	19.4	5.9
110*	−22.1	14.1	6.5
326	−20.3	5.6	7.1
500	−20.7	4.1	7.1
750	−23.1	3.2	7.9

* Indicates depths of the chlorophyll maxima at the time bulk POM samples were collected.

3.3.2. X-POM, station 8

Glycolipids: X-POM glycolipids are dominated by high relative proportions of $C_{14:0}$, $C_{16:0}$, and $C_{18:0}$ at all depths (Fig. 4b). Polyunsaturated FA (PUFA) such as $C_{22:6}$ and $C_{18:2}$ are minor components and are only present in the upper water column. The mid- to lower-OMZ is marked by a relative increase in the $C_{18:1\omega9}$ isomer (Fig. 4b). The long-chain fatty acid $C_{22:1}$ was detected exclusively in the glycolipid fraction, and it is a minor component at most subphotic depths

Phospholipids: X-POM phospholipids exhibit comparatively little diversity of fatty acids (Fig. 4d). $C_{18:0}$ and $C_{16:0}$ are the dominant components, with $C_{18:0} > C_{16:0}$ at most depths. $C_{16:1}$ also contributes significantly at all depths, particularly in the OMZ. $C_{18:1\omega7}$ and $C_{17:1}$ – both attributed most commonly to bacterial sources – are present in small proportions at all or most depths, respectively. An increased concentration of $C_{17:1}$ is observed in the mid-OMZ. PUFAs and $C_{18:1\omega9}$ are trace components only detectable in the photic zone. Similarly, $C_{12:0}$ and $C_{14:0}$ are minor or undetectable, with both peaking at the upper subphotic depth (170 m).

3.3.3. L-POM, station 8

Glycolipids: Glycolipids from L-POM show a similar profile of fatty acids as glycolipids from X-POM, but with relatively more $C_{16:0}$ and less $C_{14:0}$ at most depths (Fig. 4a). In addition PUFAs are present in L-POM throughout the water column, including mainly $C_{20:5}$ and $C_{22:6}$ at subphotic depths but with $C_{16:4}$, $C_{18:2}$, and $C_{18:4}$ also present in the photic zone. The OMZ again is marked by a relative increase in unsaturated compounds, with $C_{18:1\omega9}$ and $C_{22:1}$ peaking in the upper OMZ (274 m), and $C_{22:6}$, $C_{18:1\omega7}$, and $C_{17:1}$ peaking in the mid-OMZ (398 m; Fig. 4a). Most unsaturated compounds are minor components in the lower OMZ, but $C_{22:1}$ and $C_{22:6}$ remain in significant proportions. Just as in X-POM, $C_{12:0}$ peaks in the lower OMZ, where it is also observed that $C_{18:0} > C_{16:0}$.

Phospholipids: Phospholipids from L-POM contain fatty acid profiles similar to phospholipids from X-POM, but with the addition of significant proportions of $C_{20:5}$ and $C_{22:6}$ at most depths (Fig. 4c). In the mid-OMZ (398 m), $C_{17:1}$ and $C_{18:1\omega7}$ constitute a larger proportion relative to X-POM. Here the $C_{18:0}$/$C_{16:0}$ ratio is < 1 and $C_{18:0}$ is of lower relative abundance than in X-POM. This contrasts with the other subphotic depths, where the $C_{18:0}$/$C_{16:0}$ ratio in L-POM is > 1 and generally increases with depth.

3.3.4. Comparison to station 1

Glycolipids: The photic zone at Station 1 contains a distribution of fatty acids different from Station 8: $C_{18:0}$ is present

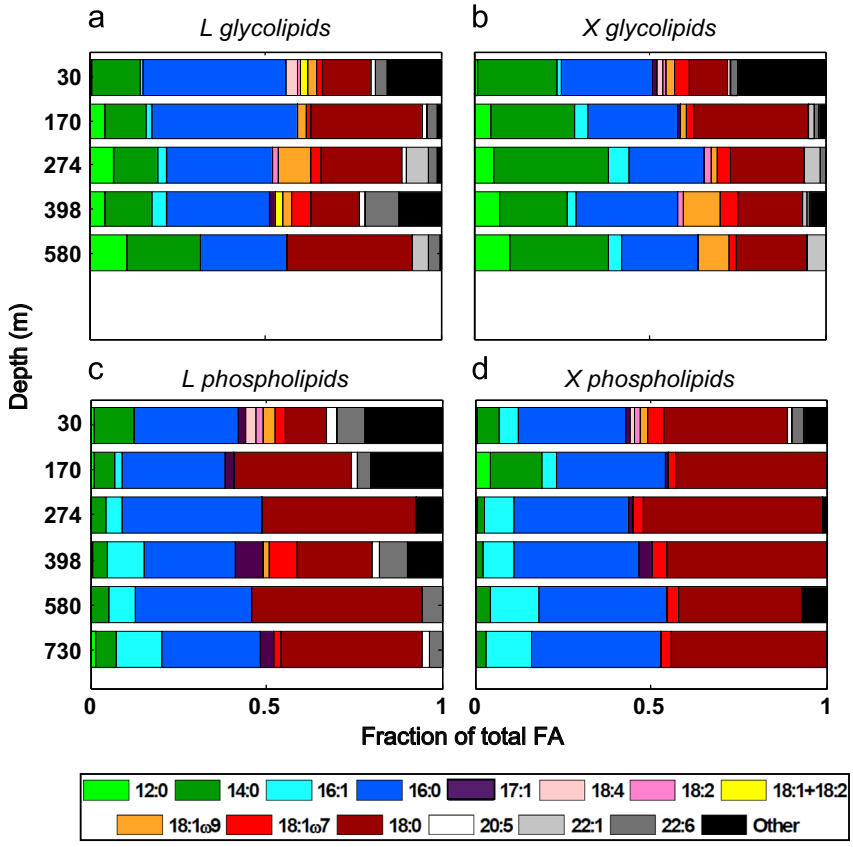

Fig. 4. Fractional contribution of 14 major fatty acids to sampling depths at Station 8, separated by size and IPL polarity fraction: (a) 0.7–53 μm (L) glycolipids; (b) 0.2–0.7 μm (X) glycolipids; (c) 0.7–53 μm (L) phospholipids; and (d) 0.2–0.7 μm (X) phospholipids. Compounds included as "other" are described in the text.

only in low concentrations, while $C_{18:4}$ and other polyunsaturated C_{18} isomers are very abundant (Fig. 5a). At the lower chlorophyll maximum, $C_{16:1}$ is the dominant glycolipid component, and $C_{18:4}$ is a trace component. Subphotic POM contains distributions of glycolipid fatty acids similar to Station 8. There is a pronounced increase in $C_{18:0}$ with depth in both size fractions, while $C_{14:0}$ decreases in concentration over the same range. The prevalence of $C_{22:1}$, $C_{18:1\omega9}$, and $C_{18:1\omega7}$ at subphotic depths is similar to Station 8.

Phospholipids: Phospholipids at Station 1 display the greatest contrast to Station 8 (Fig. 5c and d). $C_{18:0}$ comprises a much smaller portion of the total at all depths, with $C_{18:0}/C_{16:0}$ always < 1, especially in X-POM. $C_{16:1}$ instead is a prominent component at all depths and both size classes. As with Station 8, $C_{17:1}$ becomes a larger component in the OMZ, and in general, branched and odd-chain compounds become more abundant (14–20% of total fatty acids in the upper- and mid-OMZ, both size classes). Branched and odd-chain compounds are more diverse and have relative abundance up to 6 times greater in the phospholipid fraction than in the glycolipid fraction (Table 2). Two unidentified fatty acids – possibly branched $C_{15:0}$ compounds but distinct from *iso*- or *anteiso*- forms – were detected in X-POM only.

3.4. ^{13}C content: total fatty acids and POM

Within each sample, values of $\delta^{13}C$ could be determined for between 2 and 22 individual compounds (Tables 1 and 2). To compare large-scale isotopic patterns across all of the data, mass-weighted average $\delta^{13}C$ values were calculated using all measured fatty acids in each polarity class and size fraction ($\delta^{13}C_{avg}$; vertical bars, Figs. 6a and b; 7a and b). If IPLs are mainly the products of in situ, living organisms, $\delta^{13}C_{avg}$ values should reflect the aggregate ^{13}C content of the in situ community. Values of $\delta^{13}C_{avg}$ span from $-30.1‰$ to $-26.6‰$ at Station 8 and $-31.5‰$ to $-24.2‰$ at Station 1, and their depth profiles range from nearly invariant (Station 8, X-POM phospholipids; Fig. 6b) to $\sim 4‰$ deviation over < 100 m in the upper water column (Station 1, L-POM, both polarity fractions; Fig. 7a and b). L-POM exhibits the most variation in $\delta^{13}C_{avg}$ with depth, with the most negative values at the upper chlorophyll maximum at both stations and values 2.8‰ to 3.8‰ more positive in the mid-OMZ (Figs. 6 and 7). In the lower OMZ and below, values of $\delta^{13}C_{avg}$ return to more negative values.

In general, values of $\delta^{13}C_{avg}$ from X-POM are enriched in ^{13}C relative to L-POM measured at the same depths and locations (Student's *t*-test: $p = 0.014$, $n = 16$). This trend is pronounced at Station 1, where values of $\delta^{13}C_{avg}$ in X-POM are 1.5–2.3‰ more positive than L-POM (Fig. 7). At Station 8, the $\delta^{13}C_{avg}$ value for X-POM is significantly more positive than that of L-POM only in the upper water column (above 300 m; *t*-test: $p = 0.052$, $n = 6$; Fig. 6). The size-class distinction is greater in the phospholipids: in the photic zone the value of $\delta^{13}C_{avg}$ for the glycolipids from the two size classes is nearly identical ($\sim -29.5‰$); but for the phospholipids, X-POM is 2.8‰ more positive than L-POM (L: $-30.1‰$; X: $-27.3‰$). This pattern mirrors differences in compound distributions: in the photic zone, the two size classes contain very similar profiles of glycolipid fatty acids but different profiles and $\delta^{13}C$ values of specific phospholipid fatty acids (below).

In general, values of $\delta^{13}C_{avg}$ for phospholipids are more positive than those for glycolipids from the same station, depth, and size class (*t*-test: $p < 0.0002$, $n = 20$). The distinction is largest at Station 1, where values of $\delta^{13}C_{avg}$ for phospholipids in both size classes are enriched by 1.3‰ to 3.1‰ over glycolipids from the same depth

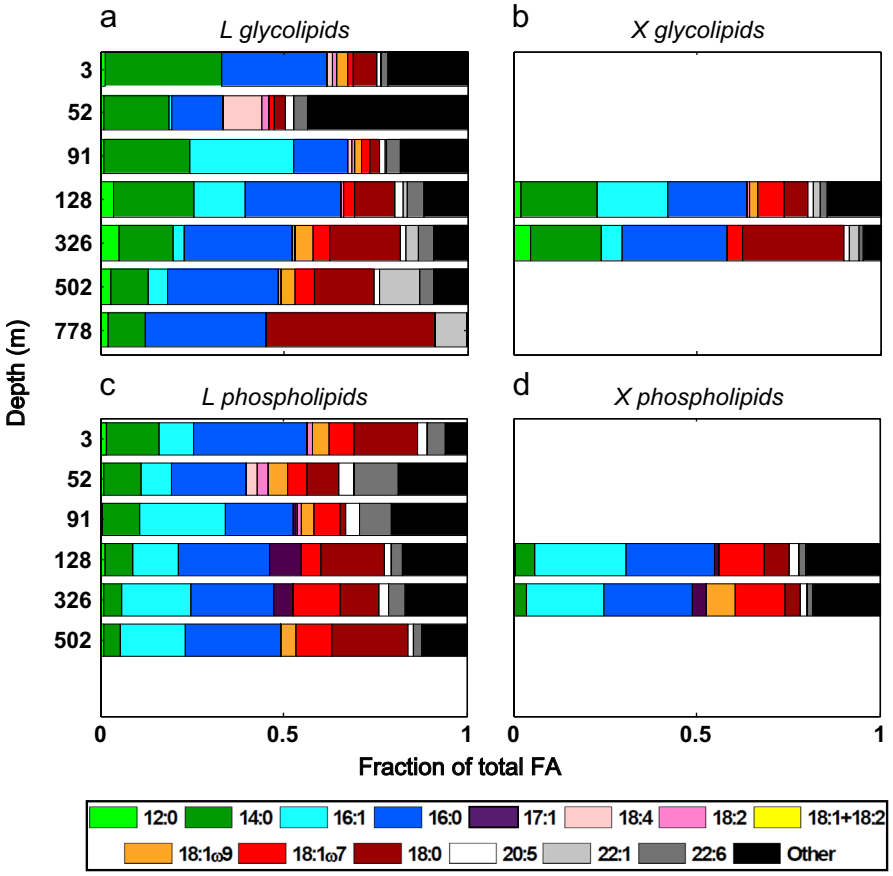

Fig. 5. Fractional contribution of 14 major fatty acids to sampling depths at Station 1, separated by size and IPL polarity fraction: (a) 0.7–53 μm (L) glycolipids; (b) 0.2–0.7 μm (X) glycolipids; (c) 0.7–53 μm (L) phospholipids; and (d) 0.2–0.7 μm (X) phospholipids. Compounds included as "other" are described in the text.

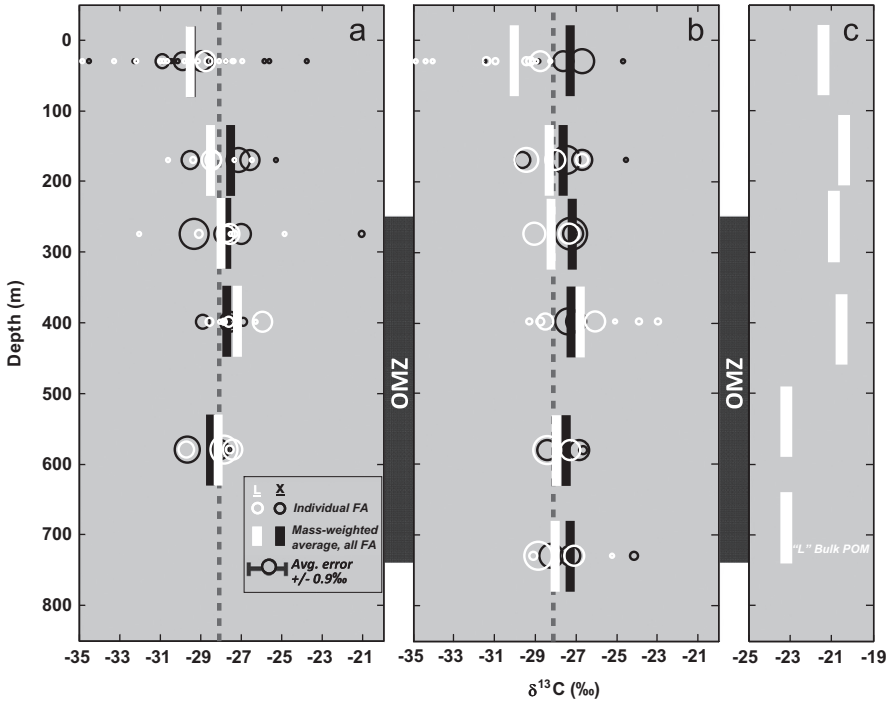

Fig. 6. (a, b) Compound-specific (circles) and mass-weighted average (vertical bars) $\delta^{13}C$ values for all measured fatty acids, Station 8, both size fractions: 0.7–53 μm (L, white) and 0.2–0.7 μm (X, black). (a) glycolipids; (b) phospholipids. Size of circles is proportional to the relative concentration of individual compounds in the sample. Vertical dashed grey line indicates the mean $\delta^{13}C$ value of all fatty acids from Station 8. In (a) 30 m X-glycolipid average values overlap directly with L-glycolipid average values. (c) $\delta^{13}C$ values for bulk POM obtained from the 0.7–53 μm size class (L); measurement error was smaller than the width of data symbols.

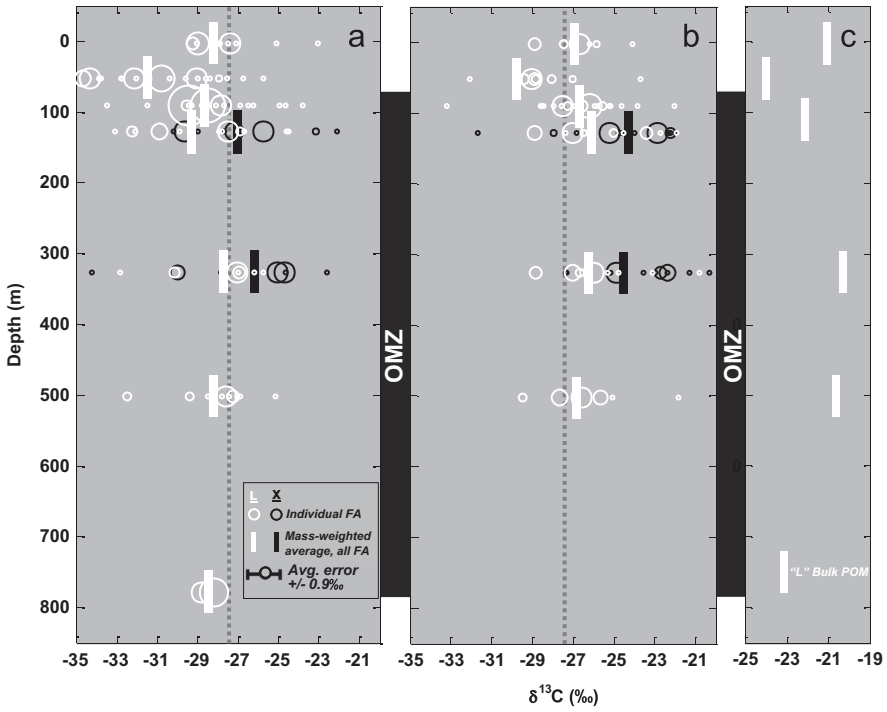

Fig. 7. (a, b) Compound-specific (circles) and mass-weighted average (vertical bars) $\delta^{13}C$ values for all measured fatty acids, Station 1, both size fractions: 0.7–53 μm (L, white) and 0.2–0.7 μm (X, black).(a) glycolipids; (b) phospholipids. Size of circles is proportional to the relative concentration of individual compounds in the sample. Vertical dashed grey line indicates the mean $\delta^{13}C$ value of all fatty acids from Station 1. Data point not shown for few compounds with $\delta^{13}C$ values $< -35‰$. (c) $\delta^{13}C$ values for bulk POM obtained from the 0.7–53 μm size class (L); measurement error was smaller than the width of data symbols.

(Fig. 7b). The largest such difference was observed in the upper OMZ.

Depth trends in the $\delta^{13}C$ value of bulk L-POM correspond to the variation observed in values of IPL $\delta^{13}C_{avg}$ from L-POM; i.e., the offset between $\delta^{13}C$ values of bulk POM and lipids varies little with depth (Table 3; Figs. 6 and 7c). At Station 8, $\delta^{13}C$ values of bulk L-POM range between $-23.2‰$ and $-20.4‰$, with the highest values at upper subphotic (170 m) and OMZ (274, 398 m) depths, and the lowest values in the lower OMZ/deep mesopelagic depths. These values are 5.0–8.1‰ and 4.8–8.8‰ more positive than $\delta^{13}C_{avg}$ values of glycolipids and phospholipids from the same depths, respectively; the offset between bulk L-POM and lipids is largest at 30 m and steadily decreases over depth. At Station 1, bulk L-POM $\delta^{13}C$ values range between $-24.0‰$ and $-20.3‰$, and are highest again at upper subphotic and OMZ depths, but lowest at the depth of the euphotic chlorophyll maximum (52 m; Fig. 7c). These values are 5.4–7.5‰ and 4.6–6.2‰ more positive than glycolipids and phospholipids, respectively, with the offset smallest at 91 m and 778 m and relatively constant at all other depths. Due to the use of carbon polymer (Supor) filters, it was not possible to measure $\delta^{13}C$ values of bulk X-POM.

3.5. *^{13}C content: Individual fatty acids*

The range in $\delta^{13}C$ values across individual compounds was much larger than the range in $\delta^{13}C_{avg}$ values, spanning from $\sim -35‰$ to $-21‰$ at Station 8 and $\sim -44‰$ to $-20‰$ at Station 1. A few major individual compounds (e.g., $C_{14:0}$ and $C_{16:0}$) clearly control the values of $\delta^{13}C_{avg}$. Both the $\delta^{13}C$ values of individual compounds and the presence or relative concentration of specific compounds vary between size classes, polarity fractions, and depths. As a result, although the general distribution of $\delta^{13}C$ values remains: X phospholipids > X glycolipids ≈ L phospholipids > L glycolipids, this pattern does not hold universally on the individual-compound level. Many of the minor compounds with outlying values, e.g., $C_{18:1\omega7}$, deviate from these average patterns (Tables 1 and 2). Individual compound data therefore likely record the diversity of IPL producers, in contrast to the aggregate community biomass represented in values of $\delta^{13}C_{avg}$.

In X-POM phospholipids at Station 8, $C_{16:0}$ and $C_{18:0}$ are highly abundant and relatively ^{13}C-enriched, thus contributing foremost to the overall ^{13}C enrichment of X-POM phospholipids relative to L-POM. Similarly, $C_{16:0}$ and $C_{18:1\omega7}$ fatty acids in both the glyco- and phospholipid fractions display ^{13}C enrichment in X-POM relative to the same compounds in L-POM at both stations (Tables 1 and 2).

Relative ^{13}C enrichment in phospholipids over glycolipids is also most evident within a few major compounds. In L-POM from the upper OMZ at Station 1 $C_{14:0}$ and $C_{16:1}$ from phospholipids are 4–6‰ enriched in ^{13}C relative to glycolipids. At Station 8, this pattern is most evident in $C_{14:0}$ and $C_{18:0}$.

Trends in individual $\delta^{13}C$ values also are observed over depth in the water column. Most compounds are relatively depleted in ^{13}C at the upper chlorophyll maximum of both stations (1–2‰ depleted compared to the same compounds at underlying depths). The C_{16} and C_{18} PUFAs contribute additionally to overall negative $\delta^{13}C_{avg}$ values at the chlorophyll maximum, as they are detected only in the photic zone and are 2–4‰ depleted compared to co-occurring compounds.

In the mid-OMZ at Station 8 (398 m), many individual compounds are ^{13}C-enriched relative to adjacent depths – a pattern which is also observed in bulk POM and $\delta^{13}C_{avg}$ values. This relative increase in $\delta^{13}C$ values is greater in L-POM than in X-POM, thereby eliminating the pattern of $\delta^{13}C_X > \delta^{13}C_L$ observed in the upper water column. In L-POM, $C_{16:0}$ and $C_{22:6}$ in all fractions, as well as $C_{18:1\omega9}$ in the glycolipids and $C_{14:0}$ in the phospholipids, all increase in ^{13}C content compared to shallower depths. The increase in $\delta^{13}C$ values is sometimes > 5‰ for these compounds between the photic zone and mid-OMZ waters (Table 1). The general ^{13}C pattern between compound classes

($\delta^{13}C_{phospho} > \delta^{13}C_{glyco}$) is recorded on the individual-compound level primarily in $C_{14:0}$ and $C_{22:6}$.

The mid-OMZ also hosts the most positive $\delta^{13}C$ values for many individual compounds at Station 1 (326 m). A relative increase in $\delta^{13}C$ value between the upper- and mid-OMZ at Station 1 is most evident in the straight-chain, saturated phospholipids of L-POM ($C_{14:0}$, $C_{16:0}$, and $C_{18:0}$) and unsaturated glycolipids of L-POM ($C_{16:1}$, $C_{18:1\omega9}$, $C_{22:1}$, and $C_{22:6}$). Here, the relative increase in $\delta^{13}C$ values of individual compounds in X-POM is again of smaller magnitude than L-POM, but the pattern of $\delta^{13}C_X > \delta^{13}C_L$ is preserved in the values of $\delta^{13}C_{avg}$ as well as in several individual compounds ($C_{16:1}$, $C_{16:0}$, and $C_{18\omega7}$, both polarity fractions).

The bacterial biomarker lipids *iso*- and *anteiso*-$C_{15:0}$ were present in sufficient abundance to measure their $\delta^{13}C$ values only in a few samples. At Station 8, these compounds were measurable only in the glycolipids from the photic zone (both X and L): here, *i*-$C_{15:0}$ was 2‰ to 4‰ enriched in ^{13}C over corresponding values of $\delta^{13}C_{avg}$ (Table 1). At Station 1 both *i*- and *a*-$C_{15:0}$ were measurable at multiple depths and were ~2‰ to 6‰ more positive than the corresponding $\delta^{13}C_{avg}$ values. Values were usually ~ −25‰ to −24‰, and as high as −22‰ to −20‰ in OMZ phospholipids (Table 2). In contrast, the two unidentified FA in the same samples (possibly isomers of branched C_{15} fatty acids) exhibited the most negative measured $\delta^{13}C$ values of this study (−44‰ to −39‰).

4. Discussion

4.1. Size distinctions in suspended POM

4.1.1. Importance of submicron POM

A size class analogous to "X-POM" (0.2–0.7 μm, i.e., exclusively submicron POM) has been collected for lipid (Brinis et al., 2004; Ingalls et al., 2012) and/or compound-specific isotopic analysis (Ingalls et al., 2006; Close et al., 2013) only on limited occasions. The living component of these submicron particles is almost exclusively prokaryotic (e.g., Koike et al., 1990; Fuhrman et al., 1989), and previous studies have treated intact polar lipids as reflecting live cells (e.g., Harvey et al., 1986; Rütters et al., 2002; Brinis et al., 2004; Sturt et al., 2004; Lipp et al., 2008; Schubotz et al., 2009; Van Mooy and Fredricks, 2010; Popendorf et al., 2011b). By this reasoning, IPLs in X-POM should reflect prokaryotes living in situ at each sampling depth. Biomass of living Archaea was likely present in X-POM (Ingalls et al., 2012), but archaeal IPLs contain ether-linked isoprenoid side chains instead of acyl side chains. Therefore, IPL-fatty acids in X-POM should represent primarily living Bacteria. IPLs in L-POM likely also reflect living cells, but in this case eukaryotic lipids will be in much greater abundances than in X-POM. Detrital (nonliving) contributions also are possible sources of IPLs in submicron and suspended POM (Schouten et al., 2010). IPLs are nonetheless more labile than bulk POM and can be considered at least a product of recent marine production.

X-POM and L-POM contain similar concentrations of IPLs, suggesting that submicron and conventional, "suspended" POM (0.7–53 μm) contain similar quantities of fresh biomass. Wakeham and Canuel (1988) found that suspended POM (> 1 μm) did not show preferential degradation relative to "sinking" POM in the ETNP; our results favor extending this conclusion to suspended POM < 1 μm. All of these classes of POM, including X-POM, contain biochemically "fresh" material and should be considered quantitatively important in active marine carbon cycling.

These results prompt a reexamination of sampling conventions. The most common operational cutoff for collecting POM has been a 0.7 μm GF/F filter (or, less commonly, a 0.1 μm membrane during tangential flow ultrafiltration; see Verdugo et al., 2004). Dissolved organic matter (DOM) is collected as the material that passes through a 0.1, 0.2, or 0.7 μm filter. Therefore, X-POM (0.2–0.7 μm) most often is collected as part of DOM or is not collected at all. Including submicron POM (< 1 μM carbon; e.g., Sharp, 1973) within DOM (> 35 μM carbon; Hansell et al., 2009) should have negligible effects on quantifying DOM, but overlooking it in the quantification of total POM has important consequences. Submicron POM includes up to 40–70% of the fresh and/or living prokaryotic biomass in the ocean (Koike et al., 1990; Altabet, 1990). Including submicron POM within DOM also obscures the potential interaction and exchange of submicron particles with larger aggregates, a potential route for the transfer of microbial biomass into sinking material (e.g., Richardson and Jackson, 2007; Alonso-González et al., 2010). The latter issue has been recognized for the colloidal size class (0.001–1 μm; Sharp, 1973; Chin et al., 1998; Wells, 1998), which sometimes overlaps with X-POM. However, X-POM is also distinct from colloids, since it is defined more narrowly on the basis of intact cellular content.

The relative contribution of submicron POM to total bulk POM remains largely unknown throughout the world ocean, mainly because submicron POM is undersampled. We could not quantify the total carbon content of bulk POM in X-POM due to the use of carbon-polymer filters; only the lipids could be quantified. Our analyses also do not address the quantitative importance of archaeal biomass within POM, which may become proportionally more important with increasing depth (e.g., Karner et al., 2001).

4.1.2. Size-related biotic distinctions

No filtering size cutoff can produce an absolute separation between prokaryotes (typically 0.1–2 μm) and Eukarya (> 0.5 μm). Here, the nominal pore size of GF/F filters (0.7 μm) implies that prokaryotic cells were likely captured in both L-POM and X-POM. Degraded POM also can form aggregates that are larger or disaggregate into particles smaller in size than the cells from which this material originated, possibly further obscuring the distinctions between the particle size classes. However, our data are consistent in suggesting we separated fresh POM by biotic type and origin. For example, PUFAs commonly attributed to Eukarya are more abundant in L-POM at all depths: $C_{20:5}$ and $C_{22:6}$ are detected in L samples by a ratio of 1:1 to 5:1 over their presence in corresponding X samples (with a single exception at Station 1, 128 m phospholipids).

The greater proportion of phospholipids in X-POM and glycolipids in L-POM may reflect coarse partitioning of bacterial heterotrophs into X-POM and phytoplankton into L-POM. The few studies addressing phylogenetic specificity of IPL head group synthesis in natural settings suggest that bacterial heterotrophs synthesize predominantly phospholipids, whereas photosynthetic bacterial and eukaryotic plankton synthesize abundant glycolipids (Harwood, 1998; Wada and Murata, 1998; Van Mooy and Fredricks, 2010; Popendorf et al., 2011a). Photosynthetic Bacteria are often ≈ 0.7 μm in diameter (e.g., Chisholm et al., 1988) and thus were likely partially captured in both L-POM and X-POM. This includes *Synechococcus* spp., which are prominent in the upper photic zone of the Costa Rica Dome (i.e., Station 8; Li et al., 1983; Saito et al., 2005). The high concentrations of glycolipids in L-POM from the photic zone thus may reflect eukaryotic phytoplankton and some fraction of bacterial phytoplankton.

Distinctions in $\delta^{13}C$ values between compounds and size classes therefore should relate to their different biotic origins. Our results suggest that membrane lipids of Bacteria on average are relatively ^{13}C-enriched, based on relatively high $\delta^{13}C_{avg}$ values in both X-POM and in phospholipids. This could reflect a systematic enrichment in ^{13}C in bacterial total cell carbon relative to eukaryotes due to differences in C fixation (autotrophs)

or metabolic ^{13}C enrichment (heterotrophs). Alternatively, it could arise from a smaller isotopic fractionation during bacterial lipid synthesis (relative to whole-cell ^{13}C content), due to differences in biosynthetic enzymes or biochemical partitioning of cellular carbon (i.e., fraction of cell lipid versus protein and carbohydrate). However, at least in one experiment, relative ^{13}C enrichment in phospholipids over glycolipids was noted within individual cultured microbial strains (Abraham et al., 1998), so this conclusion should not be overly generalized.

Our data also may reflect changing proportions of biological sources of lipids (heterotrophic and chemoautotrophic Bacteria, photoautotrophic Bacteria, Eukarya) over depth in the water column. Intense remineralization of POM by heterotrophic Bacteria in the oxycline contributes to formation and maintenance of the OMZ. Growth of this subphotic community would contribute new phospholipids to X-POM. Accordingly, X-POM phospholipids are proportionally more abundant at these depths (Fig. 3b) and contain fatty acids that are commonly attributed to Bacteria (branched and odd-chain forms, $C_{18:1\omega7}$) in higher relative concentrations than are measured in glycolipids. This again points to X-POM phospholipids as being the "most strongly bacterial" among all lipid classes obtained from POM.

Other water column studies have observed a downward shift from relative predominance of glycolipids to phospholipids in ≥ 0.7 μm POM, sometimes accompanied by variations in the $\delta^{13}C$ values of fatty acids (e.g., Schubotz et al., 2009; Wakeham et al., 2012). These patterns were also attributed to a shift from photic zone phytoplankton to subphotic heterotrophic Bacteria as in situ producers of lipids, although alternative mechanisms involving removal of phytoplankton biomass into sinking aggregates or fecal pellets and/or differential degradation rates for IPL classes also were postulated. While we cannot rule out these latter processes, our data extend previous observations to a new, open-ocean locale and recognize an important source of prokaryotic lipids within submicron POM.

4.2. Depth-related variation in sources of POM and isotopic patterns

4.2.1. Degradative effects on bulk POM versus IPLs

Our IPL results provide new insights into biosynthetic versus degradative processes affecting bulk suspended POM over depth. Bulk POM (fresh and degraded material) and IPLs (~living cells) encompass different stages of biochemical "freshness", yet their $\delta^{13}C$ values vary in tandem over most depths sampled here (L-POM, Figs. 6 and 7). Depth-related shifts in the $\delta^{13}C$ value of bulk POM previously have been interpreted as resulting from heterotrophic degradation acting in concert with particle dynamics (e.g., Jeffrey et al., 1983; Druffel et al., 2003). For example, relative ^{13}C depletion of bulk POM in the euphotic zone versus more positive $\delta^{13}C$ values in immediately underlying, subphotic waters appears to be a common pattern in the open ocean (e.g., Druffel et al., 1998, 2003; Hwang et al., 2009; ETNP – Jeffrey et al., 1983). Low $\delta^{13}C$ values in the photic zone are thought to reflect residual POM after the loss of labile, ^{13}C-enriched components (e.g., relatively ^{13}C-enriched carbohydrates and proteins) during intensive recycling by the upper ocean microbial loop.

This same pattern is present in our samples, but it is mirrored both in bulk POM and in IPLs, even though IPLs represent living organisms. At the chlorophyll maximum IPLs likely derive primarily from phytoplankton, and their $\delta^{13}C_{avg}$ values are 1–4‰ lower than in the immediately underlying depths at both stations and for most polarity and size fractions (Figs. 6 and 7). We therefore suggest that relatively negative $\delta^{13}C$ values in the euphotic zone are driven by processes of C-fixation rather than heterotrophy. This idea is supported by Redfield-like total organic *C*/*N* at the same depths (5.9–6.0; Table 3), indicating dominance of fresh biosynthetic material within bulk suspended POM.

In contrast, degradation at subphotic depths appears to alter the ^{13}C content of bulk POM and may indirectly affect the $\delta^{13}C$ values of IPLs. As bulk POC drops sharply in concentration between the upper chlorophyll maximum and upper subphotic depths (71–81% decrease; Table 3), the positive shift in its $\delta^{13}C$ value could result from (i) the replacement of ^{13}C-depleted primary POM with the biomass of heterotrophs that become relatively ^{13}C-enriched during metabolism (DeNiro and Epstein, 1978; Logan et al., 1995); and/or (ii) relative ^{13}C enrichment in the residual pool of sinking primary biomass, due to preferential reactivity of ^{12}C bonds (e.g., Sun et al., 2004). Negative shifts in $\delta^{13}C$ values of bulk POM (occurring below ~500 m) instead could reflect (iii) the preferential preservation of POM deriving from isotopically-light, recalcitrant molecules (e.g., lipids and biopolymers; Jeffrey et al., 1983; Druffel et al., 2003; Hwang and Druffel, 2003).

The $\delta^{13}C$ values of IPLs would not be affected directly by (iii), and direct effects of (ii) are unknown, but potentially minor. IPL degradation involves cleavage of the glycerol moiety either from the polar headgroup (*sn*-3 position) or by ester hydrolysis of the fatty acid side chain(s) (*sn*-1 and *sn*-2 positions; Ding and Sun, 2005; Matos and Pham-Thi, 2009). Only the latter mechanism could preferentially remove ^{12}C from the residual IPL-fatty acid pool, and it would involve a single-site fractionation (α-position carbon), likely of insufficient magnitude to affect bulk POM or the remaining IPLs. The relative importance of enzymes responsible for each mode of degradation is unknown for natural microbial communities (e.g., Logemann et al., 2011).

Instead, fractionation occurring within the bulk POM pool due to mechanism (ii) could be indirectly reflected in subphotic IPLs via option (i), if these compounds are synthesized by heterotrophic Bacteria living in situ and using bulk POM as a carbon source. Mechanism (iii), however, could gradually decouple the $\delta^{13}C$ values of bulk POM and IPLs over increasing depth (i.e., increasing degradation of the bulk POM pool). The decrease in bulk L-POM $\delta^{13}C$ values below 500 m (by ~2.5‰, both stations) is consistent with advancing degradation, perhaps related to increasing oxygen concentrations below the OMZ. IPL $\delta^{13}C_{avg}$ values do not reflect as large a depletion in ^{13}C at these depths, indicating that heterotrophic Bacteria may use the remaining ^{13}C-enriched, labile portion of bulk-POM as a substrate.

It is unclear whether heterotrophs (and/or dark autotrophs) themselves can produce amounts of biomass and distinct metabolic ^{13}C signatures sufficient to shift the $\delta^{13}C$ value of bulk POM directly (option i). In this case, correspondence between $\delta^{13}C_{avg}$ values of IPLs and POM could result from their common biological source rather than diagenetic effects. The relatively low *C*/*N* ratios of bulk POM in L-POM at all depths and at both stations (6.0–8.6, Station 8; 5.9–8.4, Station 1) could partially support such a non-diagenetic interpretation of the bulk $\delta^{13}C$ data.

Finally, it is unlikely that there is a contribution from isotopically-light exogenous terrestrial material. When examining bulk POM, advective addition of terrestrial POM can sometimes explain observations of size-related heterogeneity in $\delta^{13}C$ values (Benner et al., 1997; Sannigrahi et al., 2005). However, due to their lability, IPLs are unlikely to survive transport over long distances, and both stations in the ETNP are ~500 km from the Central American coastline.

4.2.2. Bacterial photoautotrophy

Zonation of primary producers by depth may contribute to photic zone isotopic patterns, as it is a common feature of oceanic OMZs, including the ETNP. *Synechococcus* spp. and eukaryotic

phytoplankton typically inhabit the higher-irradiance depths of the upper photic zone (ETNP; Li et al., 1983; Saito et al., 2005), while diverse *Prochloroccus* spp. thrive in the low light and low oxygen levels of the lower euphotic zone/upper OMZ ($<20\ \mu M$ O_2; e.g., ETNP, Arabian Sea, Eastern Tropical South Pacific: Goericke et al., 2000; Lavin et al., 2010). At Station 1 IPL $\delta^{13}C$ values in the upper, oxic chlorophyll maximum (52 m) are the most negative of all depths, perhaps reflecting the biosynthetic fractionation of eukaryotic phytoplankton and *Synechococcus*. In contrast, IPL $\delta^{13}C$ values are more positive in the lower chlorophyll maximum (coinciding with the upper OMZ, 91 m; Fig. 7a and b), perhaps revealing a distinctly ^{13}C-enriched signature for *Prochlorococcus*. X-POM was not sampled at 91 m, but bacterial photoautotrophs such as *Prochlorococcus* are of similar diameter to the X-L size cutoff and likely were captured partially in L-POM (Chisholm et al., 1988).

No lower chlorophyll maximum was evident at Station 8, but the relative ^{13}C enrichment of X-POM over L-POM in $C_{18:0}$, $C_{18:1\omega7}$, and $C_{16:0}$ in the upper water column (30, 170 m) may similarly reflect the biomass of ^{13}C-enriched bacterial phytoplankton and ^{13}C-depleted eukaryotic phytoplankton. Submicron cells have been identified as a major component of photic zone productivity at Station 8 (Costa Rica Dome: 20–80% of carbon fixation – Li et al., 1983; Saito et al., 2005), supporting the idea that these isotopic patterns at Station 8 reflect differences between bacterial and eukaryotic phytoplankton.

An autotrophic rather than a heterotrophic origin for relative ^{13}C enrichment in the lower photic zone at Station 1 also could provide sufficient biomass to support a non-degradative origin for the co-occurring relative ^{13}C enrichment in bulk POM (Table 3; Fig. 7c). Similar ^{13}C enrichment in X-POM relative to L-POM has been recognized in the North Pacific Subtropical Gyre (NPSG; Close et al., 2013), measured in total fatty acids rather than IPL classes. Although the NPSG results do not specify an autotrophic source for the X-POM ^{13}C enrichment, the combined observations of these two studies nonetheless suggest that submicron cells could be systematically enriched in ^{13}C relative to larger plankton throughout the ocean, i.e., there is a systematic and pre-existing isotopic difference between Bacteria and Eukarya that is not an effect of water-column or sediment diagenesis.

4.2.3. Other indicators of bacterial contribution

The relative proportions and $\delta^{13}C$ values of saturated fatty acids ($C_{14:0}$, $C_{16:0}$ and $C_{18:0}$) are different between size classes, polarity fractions, and sample depths and may represent additional distinctions between biological sources of lipids. For example, in the OMZ at both stations, phospholipid $C_{14:0}$ of both size classes has much higher $\delta^{13}C$ values (1.9–5.4‰) than glycolipid $C_{14:0}$, another possible signature of ^{13}C-rich Bacteria.

Below the photic zone, $C_{18:0}$ increases in relative abundance in both polarity fractions and size classes, leading to many depths at which the abundance of $C_{18:0} > C_{16:0}$. The $C_{18:0} > C_{16:0}$ pattern is uncommon in the water column, but it was also observed in the NPSG, in surface X-POM and in mesopelagic X-POM + L-POM (Close et al., 2013). At Station 8, high $C_{18:0}/C_{16:0}$ ratios are prominent in phospholipids and therefore could reflect bacterial synthesis. In other studies that examined total fatty acids rather than IPLs, an increase in saturated and longer-chain components instead was related directly to degradative processes, as double bonds and shorter chain-length compounds are preferentially lost (e.g., Reemstma et al., 1990). Relative increases in the concentration of $C_{18:0}$ were reported over the course of degradation experiments in which Bacteria consumed algal biomass (Harvey and Macko, 1997a) and also with increasing water column depth in the Atlantic and Pacific gyres ($>1\ \mu m$ POM; Loh et al., 2008). However, the same reasoning cannot be applied to IPLs, unless mesopelagic Bacteria selectively assimilate side chains from a partially-degraded pool as precursors for synthesis of new IPL structures.

Alternately, high relative abundances of $C_{18:0}$ previously have been attributed to zooplankton and have been considered to be a signature of "reworked" POM (e.g., Wakeham and Canuel, 1988; Wakeham, 1995). However, these studies generally examined total fatty acids from 0.7–53 μm "suspended" or > 53 μm "sinking" fractions, and not submicron material. The high abundance here of ^{13}C-enriched $C_{18:0}$ in X-POM phospholipids instead further supports bacterial production of $C_{18:0}$. If $C_{18:0}$ originated in the biomass or fecal material of mesoplankton, these materials might disaggregate and partition indiscriminately into multiple smaller size classes, and with uniform ^{13}C content. Instead, the changes in $C_{18:0}$ over depth are distinct between X-POM and L-POM. The abundance of $C_{18:0}$ also does not co-vary with other compounds generally considered eukaryotic in origin (e.g., $C_{20:5}$, $C_{22:6}$), which partition mostly into L-POM.

In contrast, the $\delta^{13}C$ values of other compounds, notably the glycolipid fatty acids (e.g., $C_{12:0}$, $C_{14:0}$), are nearly invariant with depth and size class and could represent an end-member of exported, relatively unchanged POM. Heightened preservation of intact glycolipids over phospholipids has been suggested previously in degradative experiments and models (Harvey et al., 1986; Schouten et al., 2010), but remains controversial (Logemann et al., 2011). Regardless, a source of preserved IPLs within exported particles could affect prior interpretations in which only living sources for IPLs were considered (e.g., Brinis et al., 2004; Espinosa et al., 2009; Van Mooy and Fredricks, 2010; Wakeham et al., 2012). The sources and fate of IPLs in the water column also have important implications for using IPLs to discern the provenance of sedimentary organic matter (Lipp et al., 2008; Schouten et al., 2010).

In the absence of flux measurements, it remains challenging to predict the consequences of our findings for the overall carbon budget. However, our IPL data suggest that freshly-synthesized microbial biomass from both X-POM and L-POM contribute substantially to bulk POM and may persist in sinking or slowly-settling particles, thus fueling deeper ocean microbial metabolisms.

4.2.4. Unique sources of POM in the OMZ (station 8)

The OMZ at Station 8 is marked by an increase in concentrations of IPL-fatty acids and bulk POM and a positive shift in lipid and bulk $\delta^{13}C$ values. We postulate four sources of POM that could contribute to these patterns: (a) detrital POM sinking from overlying waters, (b) biomass newly synthesized through in situ chemoautotrophy within the OMZ, (c) an "exogenous" source of detrital POM, possibly containing preserved IPLs, and (d) biomass from in situ bacterial heterotrophs in the OMZ utilizing a, b, or c as carbon sources. The "exogenous" sources in (c) could include any material that was not characterized in our analysis, namely, aggregates or organisms that were not captured in L-POM or X-POM, or which sink or migrate quickly from the surface ocean. Source (c) also could include POM advected from adjacent waters.

In the ETNP, sinking IPLs (option a) potentially could be well-preserved (Devol and Hartnett, 2001; Van Mooy et al., 2002), due to the reduced efficiency of heterotrophic respiration under low-oxygen conditions (e.g., Harvey and Macko, 1997b). However, the concentrations of most individual fatty acids (e.g., $C_{16:0}$, $C_{16:1}$, $C_{22:6}$) are higher in the OMZ in comparison to the overlying, suboxic zone, so it is unlikely that they are contributed solely by material that is passing slowly through this intermediate depth. Some fatty acids decrease in concentration in the lower OMZ and have relatively uniform $\delta^{13}C$ values at each depth (e.g., $C_{12:0}$, $C_{14:0}$,

$C_{18:0}$ in L-POM glycolipids, a possible signature of eukaryotic plankton). These compounds could represent a sinking source that is progressively degrading.

Anaerobic Bacteria and Archaea (option b) have been shown to produce new POM in many midwater OMZs (e.g., Taylor et al., 2001; Ward et al., 1989; Ward et al., 2009), including at Stations 1 and 8 in the ETNP (Podlaska et al., 2012; Rush et al., 2012). From genomic and lipid results of Podlaska et al. (2012) and Rush et al. (2012), contributions from chemoautotrophy (nitrification, anammox), along with heterotrophic denitrification, likely are concentrated in the upper and/or mid-OMZ. In the mid-OMZ, simultaneous nitrite and ammonium drawdown additionally suggest anammox activity (Podlaska et al., 2012). Wakeham et al. (2007, 2012) and Taylor et al. (2001) report similar relationships between chemoautotrophic lipids, prokaryotic cell abundance, and redox gradients in the Black Sea and Cariaco Basin.

This diversity of coexisting metabolisms in the OMZ could lead to complex mixtures of $\delta^{13}C$ values that sum to the observed positive shift in ^{13}C content in L-POM lipids and bulk POM, while also allowing for relative ^{13}C-depletion in some organisms. Mid-water carbon fixation by anammox Bacteria and bacterial nitrifiers would be expected to introduce relatively ^{13}C-depleted biomass and lipids (Schouten et al., 2004; Sakata et al., 2008). Chemoautotrophy also could partially account for the observed increase in concentrations of bulk POM and fatty acids in the mid-OMZ. Addition of biomass from anammox *Planctomycetes* would be consistent with the slightly lower $\delta^{13}C$ values in X glycolipid $C_{16:0}$ and all classes of $C_{18:1\omega7}$ observed here, although other low-oxygen microbial specialists are likely involved in these signatures as well. The majority of prokaryotic cells in the OMZ during the 2007 sampling at Station 8 were not grouped with any clades targeted by Podlaska et al. (2012), and *Planctomycetes* comprised only a small fraction. Below the OMZ, $\delta^{13}C$ values of IPLs return to values similar to the oxycline and photic zone, suggesting that the influence of the OMZ community disappears or is largely overprinted by IPLs from new material.

In contrast, studies of other oxic/OMZ transitions have revealed sharp, unidirectional isotope trends. In the upper anoxic zone of the Cariaco Basin, an abrupt decrease in the $\delta^{13}C$ value of bulk POM ($\sim$3.5‰) accompanies a sharp increase in particle concentration; both features were attributed to production by chemoautotrophs (Taylor et al., 2001; Wakeham et al., 2012). The upper OMZ in the Baltic Sea instead exhibits a large increase in $\delta^{13}C$ values of major fatty acids ($\sim$4–10‰), which was attributed to in situ carbon fixation via the reverse tricarboxylic acid (rTCA) pathway (Glaubitz et al., 2009). However, these studies did not specifically isolate submicron biomass, and therefore may not have effectively captured the metabolic and isotopic complexity of small Bacteria present in our X-POM.

Options (c) and (d) are not strictly independent from (a) and (b). Freshly-sinking large aggregates could stimulate the activity of both heterotrophs and autotrophs in the OMZ. Bacterial heterotrophs in OMZs are generally very active (option d; Lipschultz et al., 1990; Podlaska et al., 2012) and can utilize nitrite, nitrate, or sulfate to oxidize organic matter (e.g., Cline and Richards, 1972; Canfield et al., 2010). We postulate that mid-water column heterotrophs may opportunistically hydrolyze sinking, large aggregates or fecal pellets (e.g., Ward et al., 2009), potentially causing disaggregation of these large particles in excess of their in situ metabolic needs (e.g., Karl et al., 1988; Smith et al., 1992; Taylor et al., 2009). This disaggregation would introduce "exogenous" material into the suspended pools, possibly explaining the increased concentrations of multiply-unsaturated compounds such as $C_{18:2}$, $C_{20:5}$, and $C_{22:6}$ in the mid-OMZ, along with other fatty acids bearing a surface signature (option ***c***). Similarly, observations of phytoplankton-derived lipids in the mesopelagic waters of the ETNP have been linked to rapid transport and disaggregation of large aggregates (Wakeham and Canuel, 1988).

Our isotopic data add complexity to this model, since PUFAs in mid-OMZ L-POM have $\delta^{13}C$ values 2–5‰ more positive than photic zone PUFAs. Mid-OMZ PUFAs could derive from sources we have not characterized, such as mesoplankton grazers that become enriched in ^{13}C by feeding on a discrete trophic chain (DeNiro and Epstein, 1978). The mid-OMZ hosts few resident zooplankton taxa, but $\sim$15% of $>$5 mm zooplankton collected in the upper 1000 m at Station 8 were found to migrate during daytime into the low-oxygen waters of the OMZ, along with lesser proportions of smaller taxa (Wishner et al., 2013). As discussed above, the physical break-down of mesoplankton biomass or fecal pellets could supply PUFAs to L-POM, but also may be expected to create some similar particles in X-POM. However, PUFAs are relatively rare in our X-POM.

Alternatively, PUFAs in the OMZ could derive from in situ Bacteria that are ^{13}C-enriched due to their carbon uptake mechanism (e.g., rTCA cycle) or carbon substate/metabolism, reflecting options b or d. Several studies have observed capability for PUFA synthesis in Bacteria (Russell and Nichols, 1999; Shulse and Allen, 2011a, 2011b), including in anaerobes (polyketide synthase pathway: Metz et al., 2001; Kaulmann and Hertweck, 2002; Freese et al., 2008; Letzel et al., 2013) and piezophilic bacteria (Fang et al., 2006). The relative absence of PUFAs in X-POM would require that the cell size, particle-attachment, or aggregation causes the biomass of these Bacteria to be collected almost exclusively in L-POM. This interpretation may be supported by the relatively high concentration and similar $\delta^{13}C$ value of bacterial $C_{17:1}$ in L-POM phospholipids at 398 m.

The increased concentration of X-POM glycolipids in the mid-OMZ also has multiple possible origins. The possibility of substantial *de novo* production of glycolipids by subphotic Bacteria (option b or d) is largely unexplored, although heterotrophic Bacteria from surface ocean waters are known to produce glycolipids (Popendorf et al., 2011a). At mid-water depths in the Black Sea and Cariaco Basin, however, glycolipids make up only a small fraction of new IPLs synthesized by anaerobic Bacteria, contributing little *de novo* lipid to subphotic POM (Wakeham et al., 2007, 2012). The disaggregation and degradation of phytoplankton-derived sinking particles (a) could provide glycolipids to the OMZ at Station 8, but it is difficult to explain why PUFAs deriving from phytoplankton would not accompany other phytoplankton lipids injected into X-POM.

Finally, the in situ heterotrophic biomass (option d) discussed above is difficult to uniquely identify. Heterotrophic Bacteria are expected to exhibit slight enrichment in ^{13}C compared to their carbon source (e.g., DeNiro and Epstein, 1978; Blair et al., 1985; Harvey and Macko, 1997a). However, they may consume carbon deriving from multiple sources, the isotopic content of which may vary by depth and depend on the relative abundance of fresh versus degraded material. Thus, even if bacterial heterotrophs at two different OMZ depths are both denitrifiers and both synthesize the same distribution of fatty acids, their $\delta^{13}C$ values could be different. Isotopic fractionation during lipid biosynthesis, and/or effects associated with direct assimilation can also vary.

Mass-balance approaches are often employed to deconvolve mixed carbon sources. However, the biosynthetic ubiquity of IPL-fatty acids and the complexity of processes leading to isotopic patterns across size classes and polarity fractions together render it difficult to identify end-members for such an approach. Furthermore, the relative contribution of heterotrophic biomass depends on the specific production rate within the microbial community (e.g., Close et al., 2011), as well as the efficiency of conversion of substrate to heterotrophic biomass, which can vary widely (Rivkin and Legendre, 2001). Rates of heterotrophy and chemoautotrophy in depths below the photic zone have been measured at these

stations (Podlaska et al., 2012), but they do not translate directly to the standing stock of biomass or allow the relative abundance of detrital versus newly-synthesized POM to be quantified. Future work with water column models will help to decouple some of the potential complexities affecting the distribution of POM in the water column.

5. Conclusions

- Total water column concentrations of IPL-derived fatty acids from the 0.2–0.7 μm size class of POM are similar to the concentrations of these lipids measured in POM of the size class 0.7–53 μm. However, the proportional yields of glycolipids and phospholipids, the specific compound distributions, and compound-specific $\delta^{13}C$ values all are different between the size classes, indicating these fractions of POM are biologically distinct. The data point to submicron particles as a quantitatively important contributor of relatively "fresh" material – representing either living cells or recently-synthesized biomass – to total POM. We call this submicron material X-POM, or "extra-small POM".
- Up to 5‰ variation in $\delta^{13}C$ values of individual IPL-fatty acids (e.g., $C_{14:0}$, $C_{16:1}$) occurs across depth in the water column, between polar lipid classes, and/or between X-POM and larger (L) suspended POM. Because these isotopic distinctions are observed for IPLs, they are expected to represent original biosynthetic signatures and are not a direct consequence of diagenetic isotope effects. Due to physical aggregation/disaggregation processes in the water column, these isotopic differences may propagate into size fractions of sinking and/or recycled POM other than the fraction in which the signature originated.
- X-POM appears to carry a relative ^{13}C-enrichment deriving from Bacteria. IPL fatty acids from the 0.2–0.7 μm size class of POM tend to be enriched in ^{13}C in comparison to IPL fatty acids from the 0.7–53 μm size class, particularly in the upper water column. ^{13}C enrichment in X-POM IPLs could derive from expression of a smaller fractionation during fixation of inorganic carbon by bacterial autotrophs, from metabolic ^{13}C enrichment relative to substrate carbon by bacterial heterotrophs, or from enzymatic effects or cellular carbon budgets during lipid biosynthesis. This isotopic pattern is expressed more strongly in phospholipids than in glycolipids, consistent with attribution of a more "bacterial" signature to the former and a more "eukaryotic" signature to the latter.
- At the Costa Rica Dome site (Station 8) there is a net increase in the concentration of lipids and a change in the distribution and ^{13}C content of these lipids in the upper- and mid-OMZ that cannot be explained solely by uniform sinking of POM. Instead, this pattern could reflect a combination of *de novo* biomass from chemoautotrophy and an influx of suspended detrital POM from the enhanced disaggregation of large, well-preserved sinking particles. These processes likely are accompanied by additional *de novo* biomass from heterotrophs making use of both carbon sources. Together the diversity of POM sources leads to a wide range of $\delta^{13}C$ values among individual lipids in the OMZ.

Acknowledgments

We thank the crew and science party of R/V Knorr, Voyage 195, Leg 2 for technical and scientific support, particularly chief scientist Kendra Daly (USF); Monica Heintz (UCSB) for sampling and shipping advice; Steve Manganini (WHOI) and Tim Shanahan (McLane Labs) for in situ pump training; Susan Carter for cruise preparation and Meytal Higgins for receiving samples; Mary Richards and Jay Brandes (Skidaway Institute of Oceanography) for %OC, %TN, and ^{13}C of bulk POM; and Florence Schubotz and Roger Summons (MIT) for HPLC-QToF analysis of IPL headgroups. This work was supported by the National Science Foundation Grant OCE-0927290 and the Gordon and Betty Moore Foundation (to A.P.), and by an ExxonMobil Geoscience Grant (to H.G.C.). We also thank Roger Francois for editorial assistance and two anonymous reviewers for their valuable comments.

References

Abraham, W.-R., Hesse, C., Pelz, O., 1998. Ratios of carbon isotopes in microbial lipids as an indicator of substrate usage. Appl. Environ. Microbiol. 64, 4202–4209.

Abramson, L., Lee, C., Liu, Z., Wakeham, S.G., Szlosek, J., 2010. Exchange between suspended and sinking particles in the northwest Mediterranean as inferred from the organic composition of in situ pump and sediment trap samples. Limnol. Oceanogr. 55, 725–739.

Alonso-González, I.J., Arístegui, J., Lee, C., Sanchez-Vidal, A., Calafat, A., Fabrés, J., Sangrá, P., Masqué, P., Hernández-Guerra, A., Benítez-Barrios, V., 2010. Role of slowly settling particles in the ocean carbon cycle. Geophys. Res. Lett. 37, L13608, http://dx.doi.org/10.1029/2010GL043827.

Altabet, M.A., 1990. Organic C, N, and stable isotopic composition of particulate matter collected on glass-fiber and aluminum oxide filters. Limnol. Oceanogr. 35, 902–909.

Arístegui, J., Gasol, J.M., Duarte, C.M., Herndl, G., 2009. Microbial oceanography of the dark ocean's pelagic realm. Limnol. Oceanogr. 54, 1501–1529.

Bacon, M., Huh, C., Fleer, A., 1985. Seasonality in the flux of natural radionuclides and plutonium in the deep Sargasso Sea. Deep Sea Res. Part A 32, 273–286.

Bacon, M.P., Anderson, R.F., 1982. Distribution of thorium isotopes between dissolved and particulate forms in the deep sea. J. Geophys. Res. 87, 2045–2056.

Benner, R., Biddanda, B., Black, B., McCarthy, M., 1997. Abundance, size distribution, and stable carbon and nitrogen isotopic compositions of marine organic matter isolated by tangential-flow ultrafiltration. Mar. Chem. 57, 243–263.

Blair, N., Leu, A., Muñoz, E., Olsen, J., Kwong, E., Des Marais, D., 1985. Carbon isotopic fractionation in heterotrophic microbial metabolism. Appl. Environ. Microbiol. 50, 996–1001.

Bligh, E.G., Dyer, W.J., 1959. A rapid method of total lipid extraction and purification. Can. J. Biochem. Physiol. 37, 911–917.

Brinis, A., Méjanelle, L., Momzikoff, A., Gondry, G., Fillaux, J., Point, V., Saliot, A., 2004. Phospholipid ester-linked fatty acids composition of size-fractionated particles at the top ocean surface. Org. Geochem. 35, 1275–1287.

Buesseler, K.O., Lamborg, C.H., Boyd, P.W., Lam, P.J., Trull, T.W., Bidigare, R.R., Bishop, J.K.B., Casciotti, K.L., Dehairs, F., Elskens, M., Honda, M., Karl, D.M., Siegel, D.A., Silver, M.W., Steinberg, D.K., Valdes, J., Van Mooy, B., Wilson, S., 2007. Revisiting carbon flux through the ocean's twilight zone. Science 316, 567–570.

Burd, A.B., Hansell, D.A., Steinberg, D.K., Anderson, T.R., Arístegui, J., Baltar, F., Beaupré, S.R., Buesseler, K.O., Dehairs, F., Jackson, G.A., Kadko, D.C., Koppelman, R., Lampitt, R.S., Nagata, T., Reinthaler, T., Robinson, C., Robison, B.H., Tamburini, C., Tanaka, T., 2010. Assessing the apparent imbalance between geochemical and biochemical indicators of meso- and bathypelagic biological activity: what the @ $#! is wrong with present calculations of carbon budgets? Deep Sea Res. Part II: Top. Stud. Oceanogr. 57, 1557–1571.

Canfield, D.E., Stewart, F.J., Thamdrup, B., De Brabandere, L., Dalsgaard, T., Delong, E.F., Revsbech, N.P., Ulloa, O., 2010. A cryptic sulfur cycle in oxygen-minimum-zone waters off the Chilean coast. Science 330, 1375–1378.

Cass, C.J., Wakeham, S.G., Daly, K.L., 2011. Lipid composition of tropical and subtropical copepod species of the genus *Rhincalanus* (Copepoda: Eucalanidae): a novel fatty acid and alcohol signature. Mar. Ecol. Prog. Ser. 439, 127–138.

Chin, W.-C., Orellana, M.V., Verdugo, P., 1998. Spontaneous assembly of marine dissolved organic matter into polymer gels. Nature 391, 568–572.

Chisholm, S.W., Olson, R.J., Zettler, E.R., Goericke, R., Waterbury, J.B., Welschmeyer, N.A., 1988. A novel free-living prochlorophyte abundant in the oceanic euphotic zone. Nature 334, 340–343.

Cho, B., Azam, F., 1988. Major role of bacteria in biogeochemical fluxes in the ocean's interior. Nature 332, 441–443.

Cline, J.D., Richards, F.A., 1972. Oxygen deficient conditions and nitrate reduction in the eastern tropical North Pacific Ocean. Limnol. Oceanogr. 17, 885–900.

Close H.G., 2012. Size-related Isotopic Heterogeneity in Lipids from the Marine Water Column. Doctoral Dissertation, Harvard University, Massachusetts. Available from: ⟨http:/nrs.harvard.edu/urn-3:HUL.InstRepos:9789420⟩.

Close, H.G., Bovee, R., Pearson, A., 2011. Inverse carbon isotope patterns of lipids and kerogen record heterogeneous primary biomass. Geobiology 9, 250–265.

Close, H.G., Shah, S.R., Ingalls, A.E., Diefendorf, A.F., Brodie, E.L., Hansman, R.L., Freeman, K.H., Aluwihare, L.I., Pearson, A., 2013. Export of submicron particulate organic matter to mesopelagic depth in an oligotrophic gyre. Proc. Natl. Acad. Sci. 110, 12565–12570.

Codispoti, L.A., Brandes, J.A., Christensen, J.P., Devol, A.H., Naqvi, S.W.A., Paerl, H.W., Yoshinari, T., 2001. The oceanic fixed nitrogen and nitrous oxide budgets: moving targets as we enter the anthropocene? Sci. Mar. 65, 85–105.
DeNiro, M., Epstein, S., 1978. Influence of diet on the distribution of carbon isotopes in animals. Geochim. Cosmochim. Acta 42, 495–506.
Devol, A.H., Hartnett, H.E., 2001. Role of the oxygen-deficient zone in transfer of organic carbon to the deep ocean. Limnol. Oceanogr. 46, 1684–1690.
Ding, H., Sun, M.-Y., 2005. Biochemical degradation of algal fatty acids in oxic and anoxic sediment-seawater interface systems: effects of structural association and relative roles of aerobic and anaerobic bacteria. Mar. Chem. 93, 1–19.
Druffel, E.R.M., Griffin, S., Bauer, J.E., Wolgast, D.M., Wang, X.-C., 1998. Distribution of particulate organic carbon and radiocarbon in the water column from the upper slope to the abyssal NE Pacific Ocean. Deep-Sea Res. II 45, 667–687.
Druffel, E.R.M., Bauer, J.E., Griffin, S., Hwang, J., 2003. Penetration of anthropogenic carbon into organic particles of the deep ocean. Geophys. Res. Lett. 30, 14.
Espinosa, L.F., Pantoja, S., Pinto, L.A., Rullkötter, J., 2009. Water column distribution of phospholipid-derived fatty acids of marine microorganisms in the Humboldt Current system off northern Chile. Deep Sea Res. Part II: Top. Stud. Oceanogr. 56, 1063–1072.
Fang, J., Uhle, M., Billmark, K., Bartlett, D.H., Kato, C., 2006. Fractionation of carbon isotopes in biosynthesis of fatty acids by a piezophilic bacterium *Moritella japonica* strain DSK1. Geochim. Cosmochim. Acta 70, 1753–1760.
Feldman G.C., McClain C.R., Ocean Color Web, Aqua MODIS Reprocessing 32, NASA Goddard Space Flight Center. In: Kuring, N., Bailey, S.W., (Eds.), 31 January 2013. ⟨http:/oceancolor.gsfc.nasa.gov/⟩.
Fuhrman, J.A., Sleeter, T.D., Carlson, C.A., Proctor, L.M., 1989. Dominance of bacterial biomass in the Sargasso Sea and its ecological implications. Mar. Ecol. Prog. Ser. 57, 207–217.
Freese, E., Rütters, H., Köster, J., Rullkötter, J., Sass, H., 2009. Gammaproteobacteria as a possible source of eicosapentaenoic acid in anoxic intertidal sediments. Microb. Ecol. 57, 444–454.
Glaubitz, S., Lueders, T., Abraham, W.-R., Jost, G., Jürgens, K., Labrenz, M., 2009. ^{13}C-isotope analyses reveal that chemolithoautotrophic Gamma- and Epsilonproteobacteria feed a microbial food web in a pelagic redoxcline of the central Baltic Sea. Environ. Microbiol. 11, 326–337.
Goericke, R., Olson, R.J., Shalapyonok, A., 2000. A novel niche for *Prochlorococcus* sp. in low-light suboxic environments in the Arabian Sea and the Eastern Tropical North Pacific. Deep-Sea Res. I 47, 1183–1205.
Goutx, M., Wakeham, S.G., Lee, C., Duflos, M., Guigue, C., Liu, Z., Moriceau, B., Sempéré, R., Tedetti, M., Xue, J., 2007. Composition and degradation of marine particles with different settling velocities in the northwestern Mediterranean Sea. Limnol. Oceanogr. 52, 1645–1664.
Hansell, D.A., Carlson, C.A., Repeta, D.J., Schlitzer, R., 2009. Dissolved organic matter in the ocean: a controversy stimulates new insights. Oceanography 22, 202–211.
Harvey, H.R., Fallon, R.D., Patton, J.S., 1986. The effect of organic matter and oxygen on the degradation of bacterial membrane lipids in marine sediments. Geochim. Cosmochim. Acta 50, 795–804.
Harvey, H.R., Macko, S.A., 1997a. Kinetics of phytoplankton decay during simulated sedimentation: changes in lipids under oxic and anoxic conditions. Org. Geochem. 27, 129–140.
Harvey, H.R., Macko, S.A., 1997b. Catalysts or contributors? Tracking bacterial mediation of early diagenesis in the marine water column. Org. Geochem. 26, 531–544.
Harwood, J.L., 1998. Membrane lipids in algae. In: Siegenthaler, P., Murata, N. (Eds.), Lipids Photosynth.: Struct. Funct. Genet.. Kluwer Academic Publishers, Dordrecht, The Netherlands, pp. 53–64.
Harwood, J.L., Russell, N.J., 1984. Lipids Plants Microb.. George Allen & Unwin, London p. 162.
Huguet, C., Martens-Habenna, W., Urakawa, H., Stahl, D.A., Ingalls, A.E., 2010. Comparison of extraction methods for quantitative analysis of core and intact glycerol dialkyl glycerol tetraethers (GDGTs) in environmental samples. Limnol. Oceanogr.: Methods 8, 127–145.
Hwang, J., Druffel, E.R.M., 2003. Lipid-like material as the source of the uncharacterized organic carbon in the ocean? Science 299, 881–884.
Hwang, J., Montluçon, D., Eglinton, T.I., 2009. Molecular and isotopic constraints on the sources of suspended particulate organic carbon on the northwestern Atlantic margin. Deep-Sea Res. I 56, 1284–1297.
Ingalls, A.E., Shah, S.R., Hansman, R.L., Aluwihare, L.I., Santos, G.M., Druffel, E.R.M., Pearson, A., 2006. Quantifying archaeal community autotrophy in the mesopelagic ocean using natural radiocarbon. Proc. Natl. Acad. Sci. USA 103, 6442–6447.
Ingalls, A.E., Huguet, C., Truxal, L.T., 2012. Distribution of intact and core membrane lipids of archaeal glycerol dialkyl glycerol tetraethers among size-fractionated particulate organic matter in Hood Canal, Puget Sound. Appl. Environ. Microbiol. 78, 1480–1490.
Jeffrey, A.W.A., Pflaum, R.C., Brooks, J.M., Sackett, W.M., 1983. Vertical trends in particulate organic carbon ^{13}C:^{12}C ratios in the upper water column. Deep-Sea Res. 30, 971–983.
Karl, D.M., Knauer, G.A., Martin, J.H., 1988. Downward flux of particulate organic matter in the ocean: a particle decomposition paradox. Nature 332, 438–441.
Kaulmann, U., Hertweck, C., 2002. Biosynthesis of polyunsaturated fatty acids by polyketide synthases. Angew. Chem. Int. Ed. 41, 1866–1869.
Karner, M.B., DeLong, E.F., Karl, D.M., 2001. Archaeal dominance in the mesopelagic zone of the Pacific Ocean. Nature 409, 507–510.
Kawasaki, N., Sohrin, R., Ogawa, H., Nagata, T., Benner, R., 2011. Bacterial carbon content and the living and detrital bacterial contributions to suspended particulate organic carbon in the North Pacific Ocean. Aquat. Microb. Ecol. 62, 165–176.
Koike, I., Shigemitsu, H., Kazuki, T., Kazuhiro, K., 1990. Role of sub-micrometre particles in the ocean. Nature 345, 242–244.
Kostandinov, T.S., Siegel, D.A., Maritorena, S., 2010. Global variability of phytoplankton functional types from space: assessment via the particle size distribution. Biogeosciences **7**, 3239–3257.
Lavin, P., González, B., Santibáñez, J.F., Scanlan, D.J., Ulloa, O., 2010. Novel lineages of *Prochlorococcus* thrive within the oxygen minimum zone of the eastern tropical South Pacific. Environ. Microbiol. Rep. 2, 728–738.
Letzel, A.-C., Pidot, S.J., Hertweck, C., 2013. A genomic approach to the cryptic secondary metabolome of the anaerobic world. Nat. Prod. Rep. 30, 392–428.
Lewitus, A.J., Broenkow, W.W., 1985. Intermediate depth pigment maxima in oxygen minimum zones. Deep-Sea Res. 32, 1101–1115.
Li, W.K.W., Subba Rao, D.V., Harrison, W.G., Smith, J.C., Cullen, J.J., Irwin, B., Platt, T., 1983. Autotrophic picoplankton in the tropical ocean. Science 219, 292–295.
Lipp, J.S., Morono, Y., Inagaki, F., Hinrichs, K.-U., 2008. Significant contribution of Archaea to extant biomass in marine subsurface sediments. Nature 454, 991–994.
Lipschultz, F., Wofsy, S.C., Ward, B.B., Codispoti, L.A., Friedrich, G., Elkins, J.W., 1990. Bacterial transformations of inorganic nitrogen in the oxygen-deficient waters of the eastern tropical South Pacific Ocean. Deep Sea Res. 37, 1513–1541.
Logan, G.A., Hayes, J.M., Hieshima, G.B., Summons, R.E., 1995. Terminal Proterozoic reorganization of biogeochemical cycles. Nature 376, 53–56.
Logemann, J., Graue, J., Köster, J., Engelen, B., Rulkotter, J., Cypiönka, H., 2011. A laboratory experiment of intact polar lipid degradation in sandy sediments. Biogeosciences 8, 2547–2560.
Loh, A.N., Canuel, E.A., Bauer, J.E., 2008. Potential source and diagenetic signatures of oceanic dissolved and particulate organic matter as distinguished by lipid biomarker distributions. Mar. Chem. 112, 189–202.
Lomas, M.W., Moran, S.B., 2011. Evidence for aggregation and export of cyanobacteria and nano-eukaryotes from the Sargasso Sea euphotic zone. Biogeosciences 8, 203–216.
Martin, J.H., Knauer, G.A., Karl, D.M., Broenkow, W.W., 1987. VERTEX: carbon cycling in the northeast Pacific. Deep Sea Res. Part I 34, 267–285.
Matos, A.R., Pham-Thi, A.-T., 2009. Lipid deacylating enzymes in plants: old activities, new genes. Plant Physiol. Biochem. 47, 491–503.
Metz, J.G., Roessler, P., Facciotti, D., Levering, C., Dittrich, F., Lassner, M., Valentine, R., Lardizabal, K., Domergue, F., Yamada, A., Yazawa, K., Knauf, V., Browse, J., 2001. Science 293, 290–293.
Pitcher, A., Hopmans, E., Schouten, S., 2009. Separation of core and intact polar archaeal tetraether lipids using silica columns: insights into living and fossil biomass contributions. Org. Geochem. 40, 12–19.
Podlaska, A., Wakeham, S.G., Fanning, K.A., Taylor, G.T., 2012. Microbial community structure and productivity in the oxygen minimum zone of the Eastern Tropical North Pacific. Deep-Sea Res. I 66, 77–89.
Popendorf, K.J., Lomas, M.W., Van Mooy, B.A.S., 2011a. Microbial sources of intact polar diacylglycerolipids in the Western North Atlantic Ocean. Org. Geochem. 42, 803–811.
Popendorf, K.J., Tanaka, T., Pujo-Pay, M., Lagaria, A., Courties, C., Conan, P., Oriol, L., Sofen, L.E., Moutin, T., Van Mooy, B.A.S., 2011b. Gradients in intact polar diacylglycerolipids across the Mediterranean Sea are related to phosphate availability. Biogeosciences 8, 3733–3745.
Richardson, T.l., Jackson, G.A., 2007. Small phytoplankton and carbon export from the surface ocean. Science 315, 838–840.
Qi, H.P., Coplen, T.B., Geilmann, H., Brand, W.A., Bohlke, J.K., 2003. Two new organic reference materials for d13C and d15N measurements and a new value for the d13C of NBS 22 oil. Rapid Commun. Mass Spectrom. 17, 2483–2487.
Reemstma, T., Haake, B., Ittekkot, V., Nair, R.R., Brockmann, U.H., 1990. Downward flux of particulate fatty acids in the Central Arabian Sea. Mar. Chem. 29, 183–202.
Rivkin, R.B., Legendre, L., 2001. Biogenic carbon cycling in the upper ocean: effects of microbial respiration. Science 291, 2398–2400.
Rush, D., Wakeham, S.G., Hopmans, E.C., Schouten, S., Sinninghe Damsté, J.S., 2012. Biomarker evidence for anammox in the oxygen minimum zone of the Eastern Tropical North Pacific. Org. Geochem. 53, 80–87.
Russell, N.J., Nichols, D.S., 1999. Polyunsaturated fatty acids in marine bacteria—a dogma rewritten. Microbiology 145, 767–779.
Rütters, H., Sass, H., Cypionka, H., Rullkötter, J., 2002. Phospholipid analysis as a tool to study complex microbial communities in marine sediments. J. Microbiol. Methods 48, 149–160.
Saito, M.A., Rocap, G., Moffett, J.W., 2005. Production of cobalt binding ligands in a Synechococcus feature at the Costa Rica upwelling dome. Limnol. Oceanogr. 50, 279–290.
Sakata, S., Hayes, J.M., Rohmer, M., Hooper, A.B., Seemann, M., 2008. Stable carbon-isotopic compositions of lipids isolated from the ammonia-oxidizing chemoautotroph *Nitrosomonas europaea*. Org. Geochem. 39, 1725–1734.
Sannigrahi, P., Ingall, E.D., Benner, R., 2005. Cycling of dissolved and particulate organic matter at station Aloha: insights from ^{13}C NMR spectroscopy coupled with elemental, isotopic and molecular analyses. Deep-Sea Res. I 52, 1429–1444.
Schouten, S., Strous, M., Kuypers, M.M.M., Rijpstra, I.C., Baas, M., Schubert, C.J., Jetten, M.S.M., Sinninghe Damsté, J.S., 2004. Stable carbon isotopic fractionations associated with inorganic carbon fixation by anaerobic ammonium-oxidizing bacteria. Appl. Environ. Microbiol. 70, 3785–3788.

Schouten, S., Middelburg, J.J., Hopmans, E.C., Sinninghe, Damsté, 2010. Fossilization and degradation of intact polar lipids in deep subsurface sediments: a theoretical approach. Geochim. Cosmochim. Acta 13, 3806–3814.
Schubotz, F., Wakeham, S.G., Lipp, J.S., Fredericks, H.S., Hinrichs, K.-U., 2009. Detection of microbial biomass by intact polar membrane lipid analysis in the water column and surface sediments of the Black Sea. Environ. Microbiol. 11, 2720–2734.
Schubotz, F., Lipp, J.S., Elvert, M., Hinrichs, K.-U., 2011a. Stable carbon isotopic compositions of intact polar lipids reveal complex carbon flow patterns among hydrocarbon degrading microbial communities at the Chapopote asphalt volcano. Geochim. Cosmochim. Acta 75, 4399–4415.
Schubotz, F., Lipp, J.S., Elvert, M., Kasten, S., Mollar, X.P., Zabel, M., Bohrmann, G., Hinrichs, K.-U., 2011b. Petroleum degradation and associated microbial signatures at the Chapopote asphalt volcano, Southern Gulf of Mexico. Geochim. Cosmochim. Acta 75, 4377–4398.
Sharp, J.H., 1973. Size classes of organic carbon in seawater. Limnol. Oceanogr. 18, 441–447.
Shulse, C.N., Allen, E.E., 2011a. Diversity and distribution of microbial long-chain fatty acid biosynthetic genes in the marine environment. Environ. Microbiol. 13, 684–695.
Shulse, C.N., Allen, E.E., 2011b. Widespread occurrence of secondary lipid biosynthesis potential in microbial lineages. PloS One 6, e20146.
Sheridan, C.C., Lee, C., Wakeham, S.G., Bishop, J.K.B., 2002. Suspended particle organic composition and cycling in surface and midwaters of the equatorial Pacific Ocean. Deep Sea Res. I 49, 1983–2008.
Smith, D., Simon, M., Alldredge, A., Azam, F., 1992. Intense hydrolytic enzyme activity on marine aggregates and implications for rapid particle dissolution. Nature 359, 139–142.
Stramma, L., Johnson, G.C., Sprintall, J., Mohrholz, V., 2008. Expanding oxygen-minimum zones in the tropical oceans. Science 320, 655–658.
Sturt, H.F., Summons, R.E., Smith, K., Elvert, M., Hinrichs, K.-U., 2004. Intact polar membrane lipids in prokaryotes and sediments deciphered by high-performance liquid chromatography/electrospray ionization multistage mass spectrometry—new biomarkers for biogeochemistry and microbial ecology. Rapid Commun. Mass Spectrom. 18, 617–628.
Sun, M.-Y., Zou, L., Dai, J., Ding, H., Culp, R.A., Scranton, M.I., 2004. Molecular carbon isotopic fractionation of algal lipids during decomposition in natural oxic and anoxic seawaters. Org. Geochem. 35, 895–908.
Taylor, G., Iabichella, M., Ho, T.-Y., Scranton, M., Thunell, R.C., Muller-Karger, F., Varela, R., 2001. Chemoautotrophy in the redox transition zone of the Cariaco Basin: a significant midwater source of organic carbon production. Limnol. Oceanogr. 46, 148–163.
Taylor, G.T., Thunell, R., Varela, R., Benitez-Nelson, C., Scranton, M.I., 2009. Hydrolytic ectoenzyme activity associated with suspended and sinking organic particles within the anoxic Cariaco Basin. Deep Sea Res. I 56, 1266–1283.
Turley, C.M., Newell, R.C., Robbins, D.B., 1986. Survival strategies for two small marine ciliates and their role in regulating bacterial community structure under experimental conditions. Mar. Ecol. Prog. Ser. 33, 59–70.
Van Mooy, B., Keil, R.G., Devol, A.H., 2002. Impact of suboxia on sinking particulate organic carbon: enhanced carbon flux and preferential degradation of amino acids via denitrification. Geochim. Cosmochim. Acta 66, 457–465.
Van Mooy, B.A.S., Fredricks, H.F., 2010. Bacterial and eukaryotic intact polar lipids in the eastern subtropical South Pacific: water-column distribution, planktonic sources, and fatty acid composition. Geochim. Cosmochim. Acta 74, 6499–6516.
Verdugo, P., Alldredge, A.L., Azam, F., Kirchman, D.L., Passow, U., Santschi, P.H., 2004. The oceanic gel phase: a bridge in the DOM-POM continuum. Mar. Chem. 92, 67–85.
Wada, H., Murata, N., 1998. Membrane lipids in cyanobacteria. In: Siegenthaler, P., Murata, N. (Eds.), Lipids in Photosynthesis: Structure, Function and Genetics. Kluwer Academic Publishers, Dordrecht, The Netherlands, pp. 65–81.
Wakeham, S.G., 1995. Lipid biomarkers for heterotrophic alteration of suspended particulate organic matter in oxygenated and anoxic water columns of the ocean. Deep-Sea Res. 42, 1749–1771.
Wakeham, S.G., Canuel, E.A., 1988. Organic geochemistry of particulate matter in the eastern tropical North Pacific Ocean: implications for particle dynamics. J. Mar. Res. 46, 183–213.
Wakeham, S.G., Lee, C., 1989. Organic geochemistry of particulate matter in the sea: the role of particles in oceanic sedimentary cycles. Org. Geochem. 14, 83–96.
Wakeham, S.G., Amann, R., Freeman, K.H., Hopmans, E.C., Jørgensen, B.B., Putnam, I.F., Schouten, S, Sinninghe Damsté, J.S., Talbot, H.M., Woebken, D., 2007. Microbial ecology of the stratified water column of the Black Sea as revealed by a comprehensive biomarker study. Org. Geochem. 38, 2070–2097.
Wakeham, S.G., Turich, C., Schubotz, F., Podlaska, A., Li, X.N., Varela, R., Astor, Y., Sáenz, J.P., Rush, D., Sinninghe Damsté, J.S., Summons, R.E., Scranton, M.I., Taylor, G.T., Hinrichs, K.-U., 2012. Biomarkers, chemistry and microbiology show chemoautotrophy in a multilayer chemocline in the Cariaco Basin. Deep Sea Res. I 63, 133–156.
Ward, B., Glover, H., Lipschultz, F., 1989. Chemoautotrophic activity and nitrification in the oxygen minimum zone off Peru. Deep Sea Res. 36, 1031–1051.
Ward, B.B., Devol, A.H., Rich, J.J., Chang, B.X., Bulow, S.E., Naik, H., Pratihary, A., Jayakumar, A., 2009. Denitrification as the dominant nitrogen loss process in the Arabian Sea. Nature 461, 78–81.
Ward, B.B., Tuit, C.B., Jayakumar, A., Rich, J.J., Moffett, J., Naqvi, S.W.A., 2008. Organic carbon, and not copper, controls denitrification in oxygen minimum zones of the ocean. Deep Sea Res. I 55, 1672–1683.
Wells, M.L., 1998. A neglected dimension. Nature 391, 530–531.
Wishner, K.F., Outram, D.M., Seibel, B.A., Daly, K.L., Williams, R.L., 2013. Zooplankton in the eastern tropical north Pacific: boundary effects of oxygen minimum zone expansion. Deep-Sea Res. I 79, 122–140.